CHALMERS

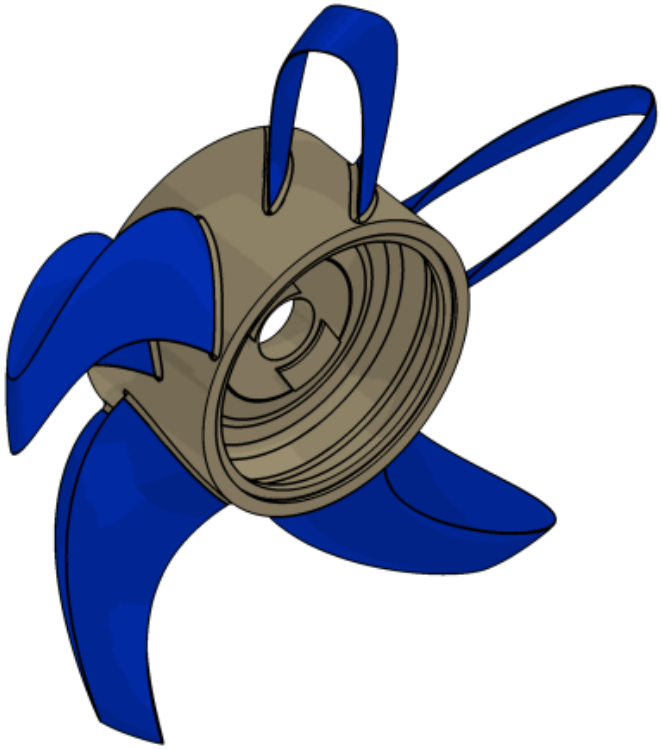

DESIGN AND TESTING OF A BOX-BLADED PROPELLER

Development of a method for aeromechanical layout

Master's Thesis in Applied Mechanics

SAMUEL ADRIANSSON

Department of Applied Mechanics
Chalmers University of Technology
Gothenburg, Sweden 2013

Master's Thesis 2013:03

MASTER'S THESIS IN MECHANICAL ENGINEERING

DESIGN AND TESTING OF A BOX-BLADED PROPELLER

Development of a method for aeromechanical layout

SAMUEL ADRIANSSON

Department of Applied Mechanics
Division of Fluid Dynamics

Chalmers University of Technology
Gothenburg, Sweden 2013

DESIGN AND TESTING OF A BOX-BLADED PROPELLER
Development of a model for aeromechanical layout
SAMUEL ADRIANSSON

Master's Thesis 2013:03
ISSN 1652-8557
Department of Applied Mechanics
Division of Fluid Dynamics
Chalmers University of Technology
SE-412 96 Gothenburg
Sweden
Telephone: +46 (0)31-772 1000

Cover:
CAD-model of a prototype box-blade geometry fitted onto a propeller hub used in physical testing

Chalmers Reproservice/Department of Applied Mechanics
Gothenburg, Sweden 2013

Abstract

Increasing oil prices and tightened environmental regulations has more and more pushed the aviation industry to focus research on the optimization of aero engines. One of the more promising technologies is the open-rotor engine, which in essence is a compromise between the good fuel economy of a turboprop and the speed and range of the turbofan. If realized in commercial aviation, the open rotor engine promises lower fuel consumption and hence less environmental impact from emissions. This concept is however still in an early design phase and thorough studies will need to be performed in order for the open rotor concept to be able to compete with the conventional aero engines of today.

As a step in the open-rotor development process, two research engineers at GKN Aerospace Engine Systems have come up with a new propeller concept for the open-rotor engine, involving so called box-bladed propellers. This concept can theoretically reduce the drag which is induced from the tip vortices created at the tip of conventional propellers. If the box-bladed propeller concept also performs satisfactory during engine operation in terms of transonic shocks and noise levels, they might well be better alternative than the conventional propeller.

This thesis has been part of a design and experimental project carried out during the fall of 2012 at GKN Aerospace Engine Systems in collaboration with the department of Fluid Dynamics at Chalmers University of Technology. The aim of the thesis work has been to develop a method for geometric, aerodynamic and mechanical layout of an arbitrary box-bladed propeller for use in small-scale model testing. The method has been developed using elementary theory of propellers, using basic aerodynamics and structural design approaches. The thesis work has resulted in a MATLAB-based design code from which a couple of propellers have been developed, analyzed and manufactured by means of Rapid Prototyping technology. The design method allows for easy changes on preliminary geometries, together with a basic aerodynamic analysis and mechanical assessment.

Keywords: *open-rotor, box-blade, high-speed propeller, propeller aerodynamics*

Acknowledgements

The present work has been performed at GKN Aerospace Engine Systems, in Trollhättan, Sweden in close collaboration with the Fluid Dynamics department at Chalmers University of Technology

First of all, I must say that this has been quite the journey with both ups and downs, but that is just like everything else in life. My thanks goes out to my collaborator Fredric Carlsvärd for his impeccable patience, support throughout the thesis and all the laughter. Furthermore, the execution of this thesis would not have been possible without the help of my supervisors Anders Lundbladh and Richard Avellán at GKN Aerospace. My deepest thanks for all the help, guidance and all the interesting discussions. I would also like to thank my examiner, professor Tomas Grönstedt at Chalmers University of Technology for his help throughout the project, valuable insights and unbeatable quotes! A special thanks to my colleagues Anna Lind, Viktor Pettersson and Johan Olofsson for their help in the review of this report.

Lastly, my warmest thanks to my family and friends for all your supports over the years. A special thanks to my grandfather Jukka, who always have fueled my engineering curiosity.

Samuel Adriansson, Gothenburg 2013-05-02

Contents

1 Introduction **1**
- 1.1 Background . . . 1
- 1.2 Objectives . . . 2
- 1.3 Limitations . . . 3
- 1.4 Brief description of the box-blade concept and relevant applications . . . 3
  - 1.4.1 The open-rotor engine . . . 3
  - 1.4.2 Intellectual property - the box-blade patent application . . . 4

2 Review of literature **7**
- 2.1 Theoretical ideas behind the box-bladed propeller . . . 7
  - 2.1.1 Non-planar wings . . . 7
  - 2.1.2 Swept wing theory . . . 9
- 2.2 Propeller basics and performance indicators . . . 10
- 2.3 Aerodynamics methods . . . 13
  - 2.3.1 Blade Element Theory . . . 13
  - 2.3.2 Actuator Disc Theory . . . 17
  - 2.3.3 BEM - combining BET and ADT . . . 20
- 2.4 Airfoil characteristics . . . 22
  - 2.4.1 NACA 16-airfoils . . . 22
- 2.5 Mechanical theory . . . 23
  - 2.5.1 Forces acting on propeller blades . . . 23
  - 2.5.2 Simple modeling of box-blade geometry . . . 24
  - 2.5.3 Bending of curved beams . . . 26

3 Method **27**
- 3.1 Box-blade geometry design method . . . 27
  - 3.1.1 The box-blade stacking line . . . 27
  - 3.1.2 Modifying the initial stacking line . . . 29
  - 3.1.3 Reference geometry generation from ADP . . . 31
- 3.2 Reference propeller aerodynamic analysis method . . . 37

3.2.1 Method development using conventional propeller and test data . . 38
3.2.2 Determining the airfoil characteristics 40
3.2.3 Correcting lift and drag coefficients 42
3.2.4 Verifying method against experimental data 43
3.3 Box-blade aerodynamic analysis method 44
3.3.1 Method development 44
3.3.2 Convergence study 47
3.3.3 Applying parameters from the reference open rotor propellers . . . 48
3.4 Box-blade mechanical analysis method 49
3.4.1 Defining mechanical reference geometry 49
3.4.2 Applying forces 51
3.4.3 Computing shear forces 52
3.4.4 Computing stresses and safety factor 52
3.4.5 Computing bending moments 53
3.5 Matlab design code 53

4 Result **55**
4.1 Aerodynamics of reference propeller 55
4.2 First box-bladed propeller results 57
4.2.1 The first and manufactured box-blade geometry 57
4.2.2 Aerodynamic performance of the first prototype 62
4.2.3 Mechanical assessment of the first prototype 65

5 Conclusion **69**
5.1 The geometrical design method 69
5.2 The aerodynamical analysis method 71
5.3 The structural assessment method 72
5.4 Recommendations for future work 72

Bibliography **76**

Appendix A - TRL stair **76**

Appendix B - Patent application abstract **78**

Appendix C - Matlab design code, main program **79**

Nomenclature

Upper-case Roman

A	Area	[m^2]
B	Number of propeller blades	[-]
C_P	Coefficient of power	[-]
C_T	Coefficient of thrust	[-]
D	Diameter of the propeller	[m]
F	Force	[N]
I	Second moment of area	[mm^4]
J	Advance ratio	[-]
P	Power	[W]
Q	Torque	[Nm]
R	Radius	[m]
T	Thrust	[N]
V	Velocity	[m/s]

Lower-case Romans

c	Sectional chord length	[m]
c_d	Sectional drag coefficient	[-]
c_l	Sectional lift coefficient	[-]
dD	Sectional drag force	[N/m]
dL	Sectional lift force	[N/m]
dQ	Sectional torque	[Nm/m]
dT	Sectional thrust	[N/m]
$\dot{m}$	Mass flow	[kg/s]
n	Rotational speed	[RPS]
p	Pressure	[N/m^2]
q	Dynamic pressure	[N/m^2]
r	Radius at given section	[m]
u	Change in velocity	[m/s]

Upper-case Greek

Λ	Sweep angle	[°]

Lower-case Greek

α	Angle of attack	[°]
β	Blade angle	[°]

γ	Convergence angle	[°]
δ	Displacement	[m]
ζ	Chord displacement angle	[°]
η	Efficiency	[-]
ϵ	Axial displacement angle	[°]
μ	Stacking line position w.r.t. leading edge	[-]
ϕ	Helix angle (advance angle)	[°]
ρ	Density	$[kg/m^3]$
σ	Stress	$[Pa]$
ω	Angular velocity	[rad/s]

Vector notation

e	Unit vector
F	Force vector
M	Moment vector
N	Axial force vector
R	Rotational matrix
V	Velocity vector
X	Coordinate matrix for e.g. stacking line

Abbreviations

ADP	Aerodynamic Design Point
ADT	Actuator Disc Theory
AF	Activity Factor
AR	Aspect Ratio
BET	Blade Element Theory
CAD	Computer Aided Design
CFD	Computational Fluid Dynamics
EOR	End-of-runway
FEM	Finite Element Method
GE	General Electric
NACA	National Advisory Committee for Aeronautics
NASA	National Aeronautics and Space Administration
SAGE	Sustainable And Green Engine
SF	Safety Factor
SNECMA	Société nationale d'études et de construction de moteurs d'aviation
TRL	Technology Readiness Level
UAV	Unmanned Aerial Vehicle
UIUC	University of Illinois at Urbana-Champaign

1

Introduction

Increasing oil prices and tightened environmental regulations has more and more pushed the aviation industry to focus research on the energy optimization of aero engines. One of the more promising technologies is the open-rotor engine, which in essence is a compromise between the good fuel economy of the turboprop and the speed and range of the turbofan. If realized in commercial aviation, the open-rotor engine promises lower fuel consumption and hence less environmental impact from emissions compared to the conventional aero engines. This concept is however still in an early design phase and thorough studies will need to be performed in order for the open rotor concept to be able to compete with the conventional aero engines of today.

1.1 Background

As a step in the open-rotor development, Anders Lundbladh and Richard Avellán at GKN Aerospace Engine Systems have come up with a new propeller concept for the open-rotor engine, involving so called box-bladed propellers instead of conventional ones. This concept can theoretically reduce the drag which is induced from the tip vortices created at the tip of conventional propellers. If the box-bladed propeller concept also performs satisfactory during engine operation in terms of transonic shocks and noise levels while maintaining a mechanical integrity, it might well be a better alternative than the conventional propeller.

However, the investigation of the box-prop concept is far from complete. During the spring of 2012, a project was conducted by students at the the Production Development department of Chalmers University of Technology [1]. The project was mainly aiming at investigating the viability of the box-bladed propeller as a future aero engine alternative in terms of the aviation market, customers, environmental- and legal regulations. A

basic structural analysis was performed in order to satisfy the stability and durability requirements of the propeller. However, the information about the aerodynamic performance of the box-blades is scarce and has a lot of development potential, making it the main focus of this thesis.

1.2 Objectives

The objective of this thesis is to develop a design method that creates a generic box-blade geometry from specified flow conditions, analyze the blade with respect to design and offdesign aerodynamics and perform a mechanical evaluation of the blade design. Furthermore, the aim is to manufacture one or a couple of prototype propellers which will be tested out in a test rig designed and built by a Fredric Carlsvärd, the second student connected to the project at GKN Aerospace. For specifics regarding the rig design, see [2]

As a basis for this master's thesis, the patent application of Anders Lundbladh and Richard Avellán [3] has been investigated in conjunction with the early design made in the Product Development project from Chalmers University of Technology [1]. A preliminary geometry is created in order to test out the manufacturing process used in the work. An improved design is then computed, using geometrical and aerodynamical data from the front rotor of an open-rotor built in the 80's. The final objective of the study is assessment of the feasibility of the box-bladed propeller as a future competitor in aero engine design. This is performed mainly from the aerodynamic and mechanical design results obtained for the manufacturing prototype and the improved geometry using GE36 data. From this, recommendations on how to proceed with the box-bladed propeller concept are stated and discussed upon.

Stating the main sub objectives more specifically, the work in this thesis is aimed at:

- Developing a method for aeromechanical layout design of a box-bladed propeller using rudimentary propeller theory.
- Investigating if the box-bladed propeller will withstand the centrifugal forces generated close to design speed without immediate changes in shape.
- Showing that a box-bladed propeller with blades swept forward will be able to operate close to design speed without catastrophic vibrations and flutter.
- Getting an initial idea on the performance of a box-bladed propeller in the low speed range, both static and dynamically (e.g. simulating a wind tunnel environment).

1.3 Limitations

Since the work performed in this thesis is at a low TRL[1], the scope of this study is constrained in order to not exceed time limits. The main limitations of the study is:

- The study is narrowed down to focus on the front rotor in the propeller arrangement, with emphasis on the actual blades. No thorough investigations has been made considering the interaction between the blades and the engine cowling, the mechanical fastening of the blades to the engine system and underlying mechanical layout.
- The elementary geometry has been created from the basis of previous studies [1], elementary theory and departmental know-how with the help of Anders Lundbladh and Richard Avellán
- Advanced three-dimensional aerodynamic analysis, e.g. CFD is not performed due to the time limit and objectives of the thesis.
- The mechanical analysis is done using elementary beam theory. No advanced numerical methods, e.g. three-dimensional FEM is performed.

1.4 Brief description of the box-blade concept and relevant applications

In this section, the engine platform suitable for the investigated propeller concept is described. Thereafter, the idea behind the box-bladed propeller is outlined with the focus mainly directed on the potential benefits of the design.

1.4.1 The open-rotor engine

The intended engine platform for the box-bladed propeller is in a high-speed propeller arrangement, making it ideal for the open-rotor engine concept. The concept was developed during the 1970s and 80s, when oil prices skyrocketed [4] and search for more efficient aero engines became a priority. In the late 80's, the oil prices dropped and reached the lowest notations in 20 years [4] and consequently, the engine companies abandoned the research. Only recently, research around the open-rotor engine has started up again with the increasing oil prices and regulations on emissions. GKN Aerospace is currently involved in a number of projects around the open-rotor engine, e.g. the SAGE1 (Rolls-Royce) and SAGE2 (SNECMA) projects in the European research program CleanSky [5]. NASA has also re-started their open-rotor research program [6].

The open-rotor concept is an engine with a similar core to that of a turbofan, but the fan has been moved from a ducted position in the front to an unducted position on the

[1] Technology Readiness Level, see Appendix A

motor cowl. The fan is generally refered to as a rotor and is mounted co-axially in pairs, a front rotor and an aft rotor. The rotors are contra-rotating with the intention that this will cancel out the swirl generated by a single rotor and direct a larger portion of airflow rearwards, producing more thrust and thus increasing efficiency. The rotor pairs can be mounted at the front of the engine cowling; a tractor configuration or further aft on the cowling in a pusher configuration as seen in Figure 1.1.

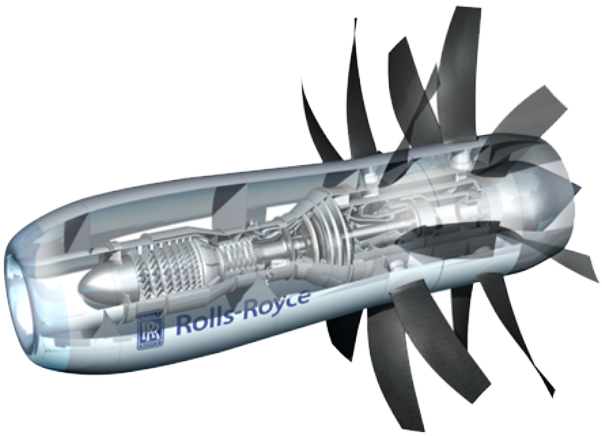

Figure 1.1: The Rolls-Royce Open Rotor Engine (Adapted from RR)

1.4.2 Intellectual property - the box-blade patent application

Research engineers Richard Avellán and Anders Lundbladh at GKN Aerospace Engine Systems has field a patent application for the box-bladed propeller, with filing date 2009-12-28 and publication date 2011-07-07 [3]. From the abstract of the patent publication, the following description concerning the invention can be read:

> *"The invention concerns an air propeller arrangement for propulsion of a fixed wing aircraft, said arrangement comprising a first air propeller that comprises a first hub member and at least a first and a second propeller blade, said first and second blades being configured to contribute significantly to said propulsion and having a substantially equal length, wherein each of said blades has an inner, root end arranged at the first hub member and an outer, tip end positioned at a distance from the first hub member such that each blade extends in a radial direction from the first hub member. The invention is characterized in that the first and second blades are interconnected at their outer ends. The invention also concerns an aircraft provided with such an air propeller arrangement."*

Conceptual sketches are provided in the patent, see Appendix B. The focus of this thesis is directed towards the front rotor of said propeller arrangement. A conceptual sketch of the box-blades mounted on an open rotor engine is shown in Figure 1.2.

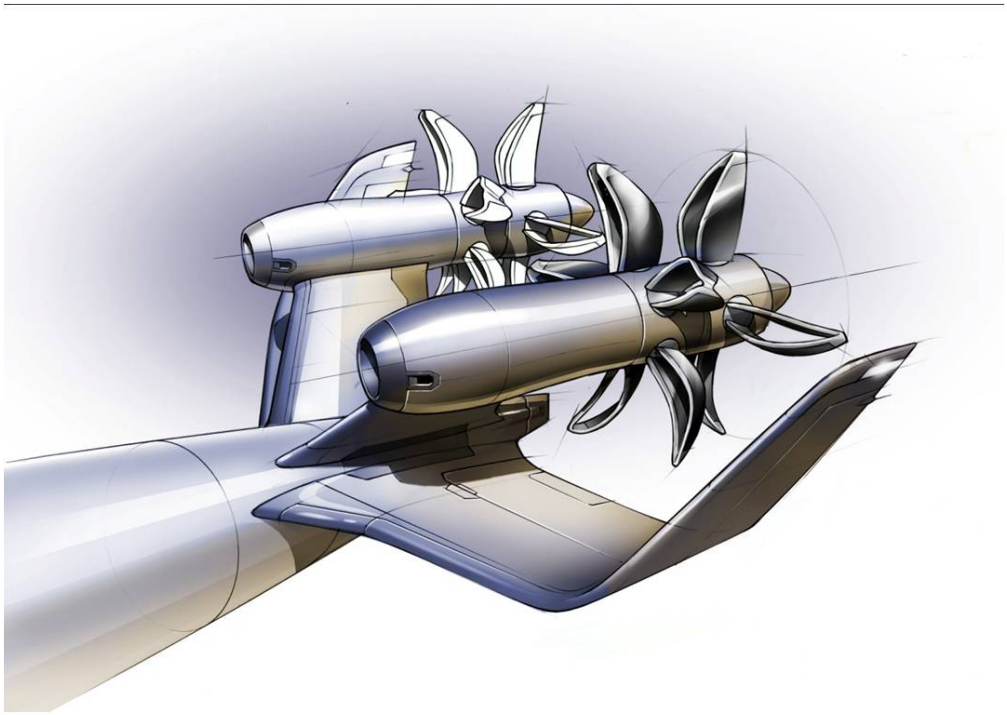

Figure 1.2: Box-bladed propeller concept (Adapted from GKN Aerospace and Chalmers)

Page left intentionally blank

2

Review of literature

The following chapter serves to summarize the literature and theories that has been reviewed prior and during the thesis work. To establish the basis for the box-blade propeller design method with main focus on the aerodynamic and mechanical analysis, it is imperative to identify relevant theories and methods. The chapter will start with a description of theoretical ideas that laid the foundation of the box-bladed concept. Next, the theories used in the aerodynamic analysis of the blade are presented. Thereafter, coefficients to determine propeller performance are described followed by an airfoil characteristics description. Lastly, theories used in the mechanical assessment of the blade are stated.

2.1 Theoretical ideas behind the box-bladed propeller

The following section serves to summarize the theories that led up to the invention and patent that has been studied in this thesis. The theory is reviewed in a somewhat more conceptual sense and has not been applied to larger extent in the actual thesis work.

2.1.1 Non-planar wings

The idea behind the box-bladed propeller originates from the non-planar wing concepts which are a hot topic regarding the future of civil aviation. Non-planar wings and multiplanes were first discussed by Prandtl [7] in the early 20th century. He concluded that there are a lot of advantages with multiplanes as compared to conventional monowing systems. One advantage of a non-planar wing configuration is that the drag can be reduced while attaining the same lift for a given planform span [8]. The drag of an airplane is made up of several components

$$C_{D,tot} = C_{D,f} + C_{D,p} + C_{D,i} + C_{D,w}$$

where $C_{D,f}$ is the *skin friction drag* caused by the boundary layers forming along the surfaces of the airplane, $C_{D,p}$ is the *pressure drag* (or form drag) originating from the shape of the airplane body , $C_{D,i}$ is the *induced drag* from the induced tip vortices and $C_{D,w}$ is the *wave drag* which appears at supersonic speeds due to the forming of compression shocks [9]. For a typical jetliner the induced drag accounts for some 40% of the total drag at cruise conditions and as much as 80% at low speeds [8]. The minimum induced drag for a planar wing can be described by the following equation

$$C_{D,i} = \frac{C_L^2}{\pi\ AR} \tag{2.1}$$

A conclusion that can be drawn is that $C_{D,i} \propto C_L^2$, meaning that the induced drag increases rapidly as the lift increases. A way to maintain a given lift while reducing the drag is increasing the aspect ratio AR (span/chord ratio) which is clear from Equation 2.1. An example of wings with high aspect ratios are found in sailplanes. However, wings with high aspect ratio becomes structurally difficult to achieve in most applications and space limitations at airports is another concern to take into account. A different way to attack the problem is by using non-planar wings, which can provide a given lift while permitting a lower aspect ratio, thus reducing the total induced drag on the wing. Various modifications of the traditional monowing are suggested by Kroo [8] to reduce the induced drag, shown in Figure 2.1 together with calculated span efficiencies. The span efficiency of each configurations is defined by the minimum induced drag of the non-planar wing divided by the minimum induced drag of a planar reference wing of the same span and lift.

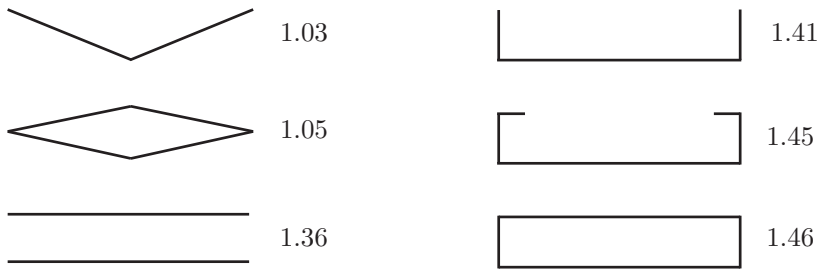

Figure 2.1: Span efficiency for various nonplanar wing configurations, with a planar monowing as reference (reproduced from [8])

From Figure 2.1, it is seen that the boxwing configuration offers higher reduction in induced drag as compared to the conventional monowing. This result is in accordance with theories that Prandtl discussed regarding the "best wing system" offering the minimum induced drag at a given lift and span [7].

Apart from aerodynamics, several other factors are of interest when it comes to non-planar wings; stability and control, strength and character of the wake vortices and structural considerations [8]. This makes the concepts particularly interesting for propeller applications. A high-speed propeller undergoes forces that may cause it to vibrate,

a phenomenon known as flutter. Applying the nonplanar wing system design for propellers, e.g. the boxwing configuration, shows obvious structural advantages; it provides a more rigid construction which is less likely to flutter. Furthermore, it provides the possibility to introduce forward sweep.

2.1.2 Swept wing theory

The critical Mach number for a straight wing or propeller blade can be related to the lowest critical Mach number of a section along the wing or blade [10]. With a sweep angle applied to the wing or blade, the effective critical Mach number can be increased, allowing for higher speeds. The wing can be swept with a positive angle meaning that the wing tips will be positioned downstream of the wing roots, also called backwards sweep. The same effect can be achieved using negative angle, or forward sweep [10].

In 1935, a German scientist named A. Busemann showed that for an infinitely long wing with backwards sweep, the aerodynamics are mainly dependent on the velocity component $V_\infty \cos^2 \Lambda$ normal to the leading edge, with Λ being the sweep angle [10]. Conversely, the component $V_\infty \sin \Lambda$ has no effect on the pressure distribution. From this, the conclusion was that for an idealized wing or blade, the critical Mach number is dependent on the velocity component $V_\infty \cos \Lambda$, which is lower than the flight speed V_∞

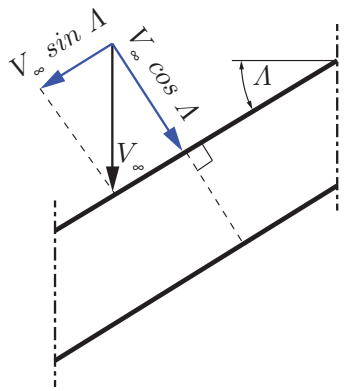

Figure 2.2: Section of a wing showing the principle of sweep (reproduced from [10])

There are however drawbacks with swept wings. For a swept wing, the lift coefficient and also the maximum lift for a given section is reduced by a factor $\cos \Lambda$ [10]. Swept wings also have a tendency to pitch-up when stalled. Furthermore, for a given span the structural length increases, increasing the weight of the wing structure, As a result, the choice of sweep angle is always a compromise. A typical sweep on a transonic jet airliner is such that the maximum cruise speed yields a velocity component normal to the quarter-chord line of approximately Mach 0.7 [10].

For the box-bladed propellers, sweep is a factor of great importance because of the desire to use the invention in high-speed application. It is easy to see that the box-bladed design provides a structurally more rigid construction compared to conventional propeller blades, which may permit the blades to be swept with larger angles compared to conventional propellers. However, since the aerodynamic effects of sweep are more prominent close to transonic speeds they are not investigated further in this thesis. The test geometries are nonetheless built with a swept shape, mainly to study the structural rigidity of the blades regarding effects of flutter in the low speed range.

2.2 Propeller basics and performance indicators

The function of a propeller in airplane applications is to displace the air and generate thrust. Propeller-driven aero engines are one of the most efficient engines in terms of fuel consumption, particularly the turboprop engine. Propellers have been used in aviation since the days of the Wright brothers[1] and the methodology for analyzing conventional propellers are well developed.

To assess the performance of propellers at various operating conditions, it is favorable to use quantities that are dimensionless. The first and foremost parameter in the non-dimensional analysis of propellers is the *advance ratio* J [10]

$$J = \frac{V_\infty}{ND} \tag{2.2}$$

with V_∞ Forward airspeed of the propeller
N Rotational speed
D Diameter of the propeller

The advance ratio signifies the ratio between the distance a propeller moves forward during one revolution compared to the diameter, the helix the propeller tip will follow during one revolution [11]. A high advance ratio indicates that the propeller is moving fast through the air while a low advance ratio means that the propeller moves slowly.

Propeller performance can then be expressed in terms of the advance ratio. Using dimensional analysis, propeller thrust, propeller power and the torque can be made non-dimensional [10] [12].

[1] Beginning of the 20th century

$$C_T = \frac{T}{\rho\, N^2\, D^4} \tag{2.3}$$

$$C_P = \frac{P}{\rho\, N^3\, D^5} \tag{2.4}$$

$$C_Q = \frac{Q}{\rho\, N^2\, D^5} \tag{2.5}$$

Expressing the performance in terms of the advance ratio has advantages in model testing. The advance ratio is not only a measure of the propellers advancement through the air, but also a scaling parameter. In essence, this means that propellers with the same J and with geometrical similarity have the same performance index [11]. This means that a large propeller at a certain rotational speed can be compared with a small scale model propeller with the same geometry using the previously defined non-dimensional parameters.

The propeller efficiency will define optimum operating points for a given propeller [10]. The efficiency can be derived from the non-dimensional coefficients defined in Equations 2.2 through 2.5. In words, the efficiency is defined as the ratio of the useful propulsive power generated by the propeller divided by the breaking power supplied to the propeller shaft by the resistance torque. When flying steady at a constant speed, the breaking power is equal to the power supplied to the propeller shaft [10]

$$\eta_{propeller} = \frac{\text{Useful propulsive power}}{\text{Shaft power in}} = \frac{T\, V_\infty}{Q\, \omega} = \frac{T\, V_\infty}{P}$$

which in turn can be made non-dimensional by using Equations 2.2, 2.3 and 2.4.

$$\eta_{propeller} = \frac{T\, V_\infty}{P} = \frac{(C_T\, \rho n^2 D^4)\, V_\infty}{(C_P\, \rho n^3 D^5)} = \frac{C_T}{C_P} \frac{V_\infty}{nD} = J \frac{C_T}{C_P} \tag{2.6}$$

From this, it is possible to compare the performance of various propellers with varying diameters, undergoing different operating conditions. The coefficients can be tabulated, generating performance charts for a given propeller.

It is easily realized from Equation 2.6 that the efficiency will go to zero as the advance ratio (airspeed) approaches zero. This is not true in reality, since the propeller will produce thrust when stationary and therefore have a measurable efficiency. In order to assess static performance of a propeller, the efficiency equations must be redefined.

Consider Figure 2.3 which depicts the stream tube around a propeller.

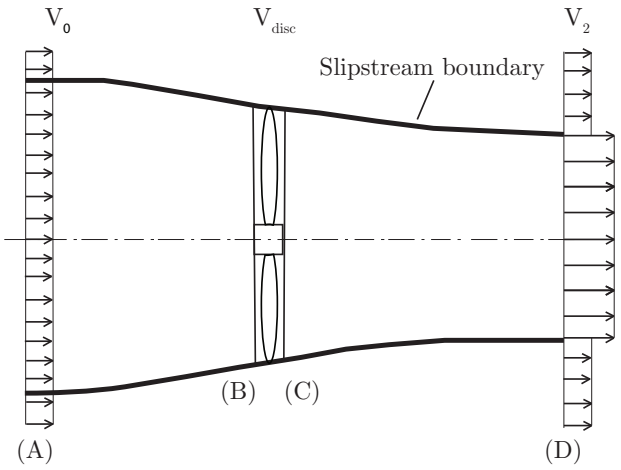

Figure 2.3: Actuator disc theory sketch

Suppose the advance ratio defined at the propeller disc is called J_{ind}, using the same definition as for the conventional advance ratio defined in Equation 2.2 but with the velocity taken at the propeller disc.

$$J_{ind} = \frac{V_{disc}}{ND} \tag{2.7}$$

Then the efficiency can be expressed in the form of the energy ratio added at the propeller disc, given by the velocity change over the propeller disc [10]

$$\eta_{ind} = \dot{m}\left(\frac{V_2^2}{2} - \frac{V_0^2}{2}\right) \; / \; P \tag{2.8}$$

Identifying three stations in Figure 2.3; one far upstream of the propeller disc (A), one at the propeller disc (B and C) and one far downstream of the propeller disc (D). The velocity increase at station B and C are equal and named u'. Far downstream of the rotor, the velocity increase is given the name u

$$V_{disc} = V_0 + u'$$
$$V_2 = V_0 + u$$

Using

$$V_2 = V_0 + u = V_0 + 2u' = V_0 + 2(V_{disc} - V_0)$$
$$\text{and} \quad \dot{m} = \rho V_{disc} A_{disc}$$

Equation 2.8 is written

$$\eta_{ind} = \rho\ V_{disc}\ A_{disc} \left(\frac{(V_0 + 2(V_{disc} - V_0))^2}{2} - \frac{V_0^2}{2} \right)\ /\ P$$

Expanding the expressions and simplifying:

$$\eta_{ind} = \rho\ V_{disc}\ A_{disc} \left(\left[\frac{(V_0^2 - 4V_{disc}V_0 + 4V_{disc}^2 - V_0^2}{2} \right] \right)\ /\ P$$

Factorizing and simplifying further yields:

$$\eta_{ind} = 2\ \rho\ V_{disc}^2\ A_{disc}\,[V_{disc} - V_0]\ /\ P \tag{2.9}$$

Remembering that $T = \dot{m}\ 2u' = 2\ \rho\ V_{disc}\ A_{disc}\,(V_{disc} - V_0)$ it is easy to identify from Equation 2.9 that:

$$\eta_{ind} = \frac{V_{disc}\,T}{P} = J_{ind}\frac{C_T}{C_P}$$

making it possible to quantify the efficiency of a propeller in terms of energy added to the jet at static conditions.

2.3 Aerodynamics methods

In this section, the aerodynamic analysis methods used for the aerodynamic assessments of the box-bladed propeller geometry are presented.

2.3.1 Blade Element Theory

A relatively easy way to predict the performance of a propeller or wind turbine rotor is using *Blade Element Theory*. The theory consists of slicing the propeller blade into a discrete number of sections along the radius of the blade. The sections are considered independent of each other. By then applying a force balance with lift and drag forces for each section, which can be translated into thrust and torque, the contribution from each blade section can be computed. Integrating this over the blade radius will then give the total propeller blade forces, which is used to assess the total performance of the propeller [10]. There are a number of assumptions made for this theory, the main being:

- Each blade element is thought of as isolated and does not affect any adjacent blade elements.
- Standard airfoil characteristics can be applied for each blade element.
- The flow conditions are assumed to be favorable. The theory will not hold when a big portion of the blade is stalled etc.

The theory does not consider 3D flow effects, such as induced flow by shed tip vorticies and radial components of the flow. This means that the method neglects a lot of real world flow features. The method will generally overpredict the propeller thrust and underpredict the propeller torque, which will result in a higher efficiency compared to experimental/measured propeller performance [13]. Figure 2.4 depicts an arbitrary propeller blade with a set of sectional profiles shown.

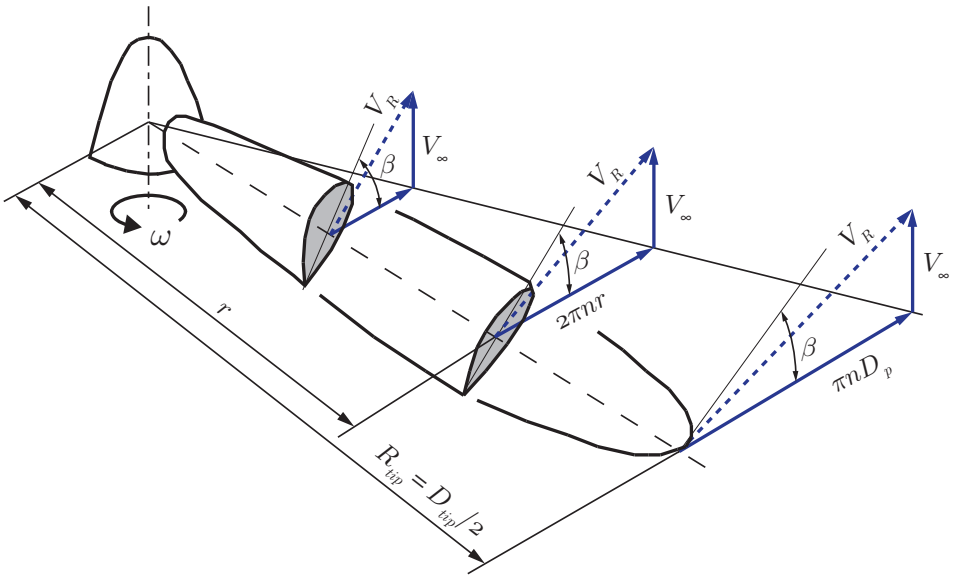

Figure 2.4: Radial subdivision of an arbitrary propeller blade (reproduced from [10])

For an arbitrary cross-section along the radius the propeller the local velocity from the relative flow at a certain profile can be divided into two components; the pure translational velocity defined by the flight speed V_∞ and a peripheral velocity from the propeller rotation $V_{rot} = \omega r$. The relative velocity, V_R, is the vector sum of the translational and peripheral velocities [10].

The relative flow makes an angle with the rotational plane, the *helix angle* ϕ (sometimes also referenced to as the advance angle). This angle is geometrically described by the helix on which a certain section of the blade advances through the air. Furthermore, the local blade section makes an angle between the relative velocity and the sectional chord, the angle of attack α. The sum of the helix angle and angle of attack make up the blade angle, defined as β, which is the total angle the blade section makes with respect to the rotational plane [10]. This particular helix on which the propeller will travel through the air is called the *geometric pitch* and can be seen in Figure 2.6. Figure 2.5 shows the velocity triangle and forces acting on a sectional blade element.

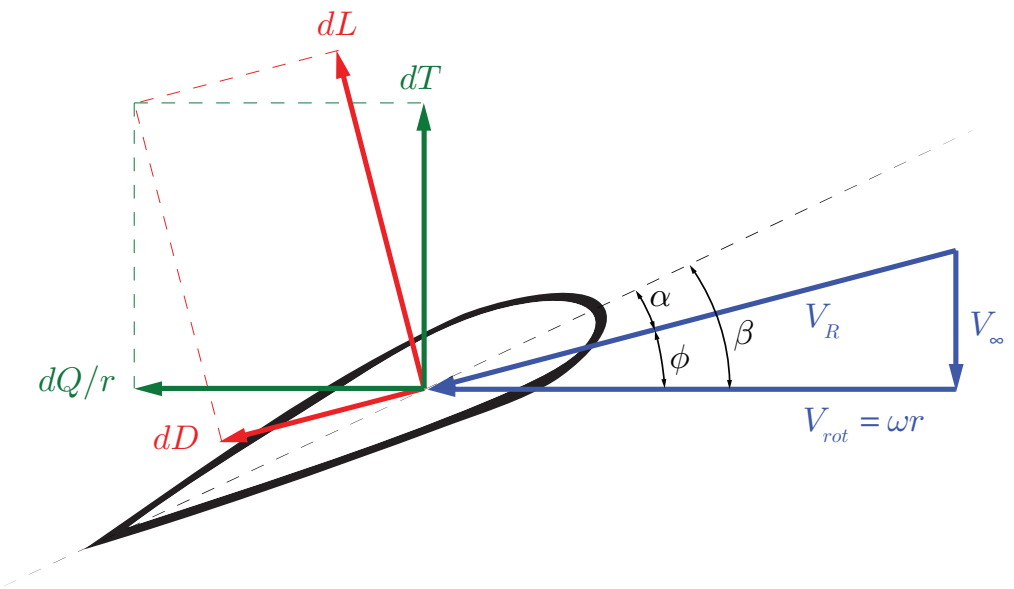

Figure 2.5: A blade element with velocity triangle and force balance

The aerodynamic forces acting on the blade element is defined by the lift force dL and the drag force dD acting on the given section. These force contributions can be integrated to find total forces acting on the blade. The contributions from lift and drag forces acting on the section can be translated into sectional thrust dT and sectional torque dQ, which when integrated gives the total thrust and torque acting on the propeller blade [13]. The contributions to thrust and torque from the lift and drag forces are given by:

$$dT = dL\cos(\phi) - dD\sin(\phi) \tag{2.10}$$

$$dQ = [dL\sin(\phi) + dD\cos(\phi)]\, r \tag{2.11}$$

The sectional lift and drag forces can be translated into non-dimensional coefficients or airfoil characteristics, which in many cases are tabulated for a given airfoil profile family and flow case [14]. This makes it possible to derive the force balance of the blade element using specific airfoil characteristics. The dimensionless lift and drag coefficients are readily written:

$$c_l = \frac{dL}{q_{rel}\; c\; dr} \tag{2.12}$$

$$c_d = \frac{dD}{q_{rel}\; c\; dr} \tag{2.13}$$

with	dL, dD	Sectional lift and drag force
	q_R	Dynamic pressure, defined as $\frac{1}{2}\rho V_R^2$
	c	Sectional chord length

Using Equations 2.12 and 2.13, Equations 2.10 and 2.11 can be rewritten:

$$dT = q_R \left[c_l \cos(\phi) - c_d \sin(\phi)\right] \; c \; dr \tag{2.14}$$

$$dQ = q_R \left[c_l \sin(\phi) + c_d \cos(\phi)\right] \; c \; r \; dr \tag{2.15}$$

Applying Equations 2.14 and 2.15 on a number of blade sections, the total thrust and torque produced by the blade can be found through integration over the relevant span of the blade (the force producing portion), ranging from the propeller hub to the tip. By multiplying with the total number of blades B, the total performance of the propeller is found.

$$T = \; B \int_{Rhub}^{Rtip} q_R \left[c_l \cos(\phi) - c_d \sin(\phi)\right] \; c \; dr \tag{2.16}$$

$$Q = \; B \int_{Rhub}^{Rtip} q_R \left[c_l \sin(\phi) + c_d \cos(\phi)\right] \; c \; r \; dr \tag{2.17}$$

The power requirement of the propeller at steady flight speed can be calculated using the integrated torque

$$P = Q\omega \tag{2.18}$$

Introducing induced velocities in the BET method

The flow case depicted in Figure 2.5 is simplified and would only be true if the propeller did not affect the air passing the blades. In reality, the blades will *induce* velocities due to the energy added by the propeller blades. To maintain the flow momentum, the speed will increase when passing the propeller blades. Locally, this will decrease the propellers advance through the air meaning that the actually pitch will be lower than the geometric pitch defined in Section 2.3.1. The actual pitch caused by this "propeller slip" is termed the *effective pitch*.

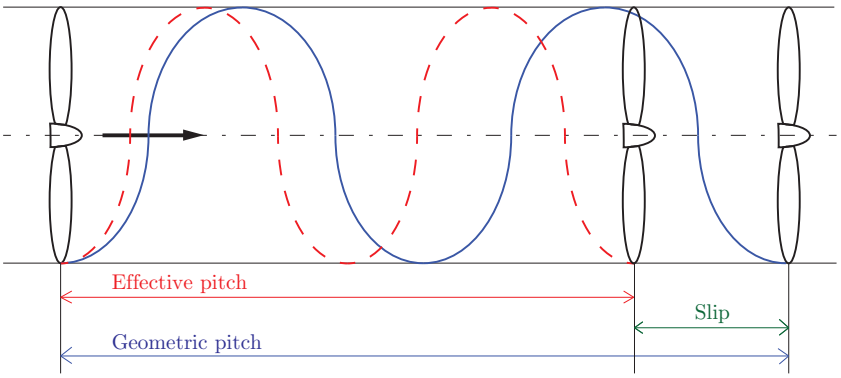

Figure 2.6: Geometric and effective pitch of a propeller

Due to the change in propeller pitch, the angle of attack changes due to the induced velocities. This suggests that the effective angle of attack is reduced by the induced velocities. The angle of attack can be divided into two components, the *induced* angle of attack α_{ind} and the *effective* angle of attack α_{eff}.

$$\alpha_{eff} = \alpha - \alpha_{ind}$$

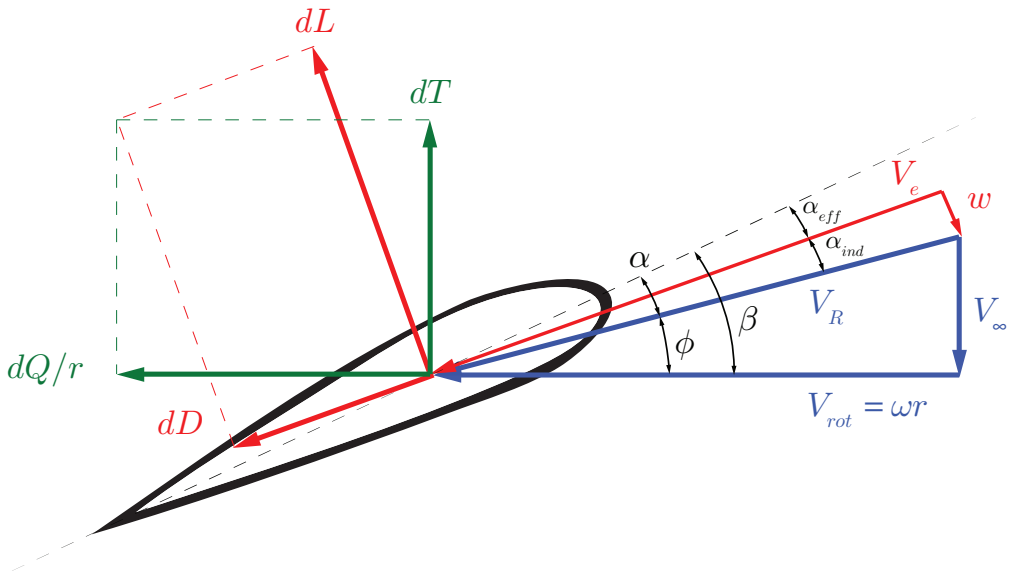

Figure 2.7: Blade element with velocity triangle and force balance, with induced velocities included

This will yield an effective relative velocity (V_e in Figure 2.7) which has the angle α_{eff} with respect to the chord line of the profile. The total change in rotational and axial velocity is expressed as w, and is made up of two components:

- Axially induced velocity, $V_{ind,axial}$
- Rotationally induced velocity, $V_{ind,rot}$

2.3.2 Actuator Disc Theory

Initially formulated by W. J. M. Rankine and W. Froude for the purpose of analyzing ship propellers, *Actuator Disc Theory* or *Momentum Theory* is a good tool for a first estimation of the flow changes around a propeller [10]. The theory is not only used in the design of ship and air propellers, but also for wind turbine rotors. A number of assumptions are made when using Actuator disc theory [15]

1. The disc is thought of as infinitesimally thin, hence giving no resistance to passing fluid. This means that frictional forces are small and negligible compared to pressure changes and momentum flux.
2. Velocity and thrust loads are uniform over the disc.
3. The pressures far upstream and downstream of the rotor are equal, given by p_∞
4. The flow is considered as inviscid, incompressible and isentropic.

The propeller is imagined to have an infinite number of blades, hence forming a solid disc. The propeller disc has an area A_{disc} and advances through the air with a velocity V_0. The thrust of the propeller can be expressed as the change in flow momentum over the stream tube region, essentially meaning the change in velocity from a point far upstream of the disc and a point far downstream of the disc [10]. The velocity is assumed to vary continuously through the control volume, while the pressure will have a discontinuity at the propeller disc. A schematic model of the actuator disc theory together with pressure and velocity distributions taken at the mean line is seen in Figure 2.8.

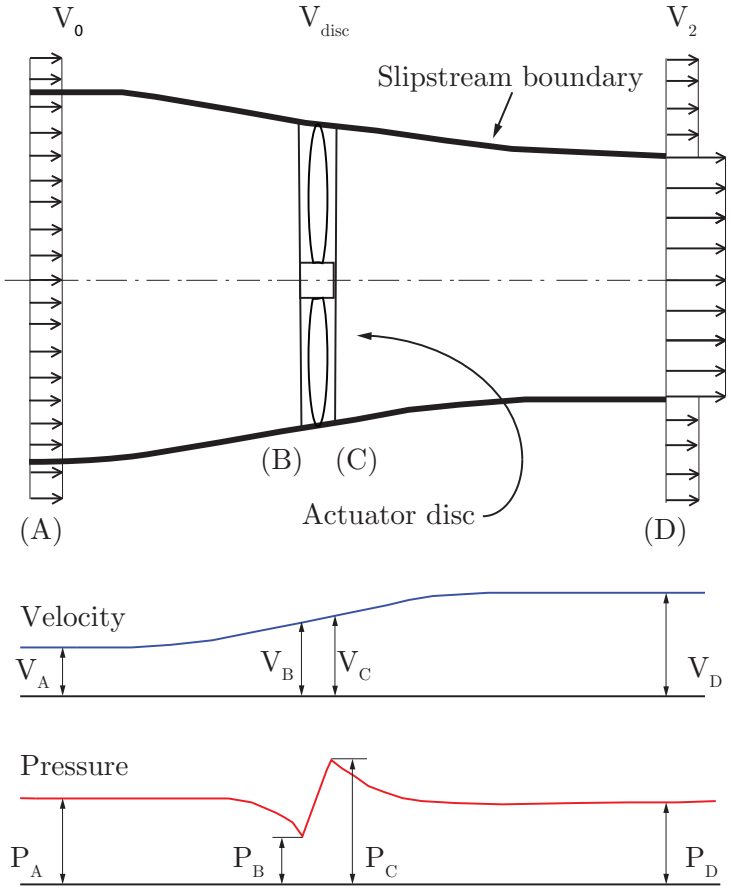

Figure 2.8: Actuator disc theory sketch with pressure and velocity distributions

If the energy is added to the flow at the propeller disc, the total head upstream of the disc and the total head downstream of the disc is constant [10]. This is not valid through the disc, since energy is added to the flow. The difference in head across the disc represents the pressure rise due to thrust since there is no change of velocity through the infinitesimally thin disc [16]. Observing a control volume surrounding the actuator disc

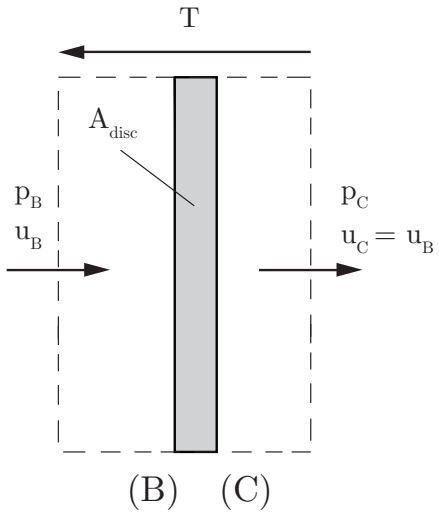

Figure 2.9: Control volume for the infinitesimally thin actuator disc

The force, in this case thrust, exerted on the disc can be written:

$$T = A_{disc}(p_C - p_B) \tag{2.19}$$

Since the assumption of incompressible flow is done [15], Bernoulli's equation is applicable upstream and downstream of the propeller.

$$\text{Upstream: } p_B + \frac{1}{2}\rho V_B^2 = p_\infty + \frac{1}{2}\rho V_0^2$$
$$\text{Downstream: } p_C + \frac{1}{2}\rho V_C^2 = p_\infty + \frac{1}{2}\rho V_2^2$$

Given that $V_B = V_C = V_{disc}$, the pressure difference over the disc can be written

$$p_C - p_B = \frac{1}{2}\rho(V_2^2 - V_0^2)$$

Inserting the result into Equation 2.19

$$T = A_{disc}\,\frac{1}{2}\rho(V_2^2 - V_0^2) = \rho\, A_{disc}\,\frac{1}{2}(V_2 + V_0)(V_2 - V_0) \tag{2.20}$$

The thrust may also be written as the change in flow momentum over the disc [10]

$$T = \dot{m}u = \rho A_{disc} V_{disc}\, u = \rho A_{disc}(V_0 + u')\, u$$

With $u' = V_{disc} - V_0$ and $u = V_2 - V_0$, Equation 2.20 is written

$$T = \dot{m}u = \rho\, A_{disc}\, V_{disc}\, u = \rho A_{disc} V_{disc}\, (V_2 - V_0) \tag{2.21}$$

Comparing the two expressions for thrust from Equations 2.20 and 2.21, the velocity at the disc can be identified

$$V_{disc} = \frac{1}{2}(V_2 + V_0)$$

suggesting that V_{disc} is the mean velocity of the far upstream and downstream velocities. From this, the conclusion is that the the velocity increase at the propeller disc is half of the total increase in the far downstream wake [10].

$$u' = \frac{1}{2}u$$

This is an important result, since the area of the propeller disc is known and hence the axial momentum at the disc can be calculated. A balance of axial momentum can then be used together with a blade element forces calculated from BET to approximate the axially induced velocity at the propeller blades.

2.3.3 BEM - combining BET and ADT

As mentioned in Section 2.3.2, integrating the local blade force contributions using BET is not enough since there is no information about the magnitude of the induced velocities. Through actuator disc theory, it is possible to define the balance of axial and angular momentum using the induced velocities. This will yield a system of equations which are solvable through iteration. For the flow cases studied in this report, the rotational part of the induced velocities is neglected for reasons of simplification. It is done with the assumption that the induced rotational velocity has a minor impact on the result when analyzing a single propeller. Neglecting the angular momentum balance will also speed up the iteration process. The penalty of this will be an increase in efficiency which is not consistent with reality, but if the assumption that the induced velocity in the axial direction is greater than the induced velocity in the rotational direction holds the assumption should be adequate for a first estimation of propeller performance.

By neglecting the induced velocities in the rotational direction the BET velocity diagrams will be slightly modified. The exclusion of the rotational component in w will decrease the induced angle of attack, giving a larger effective angle of attack. The modified flow case is depicted in Figure 2.10.

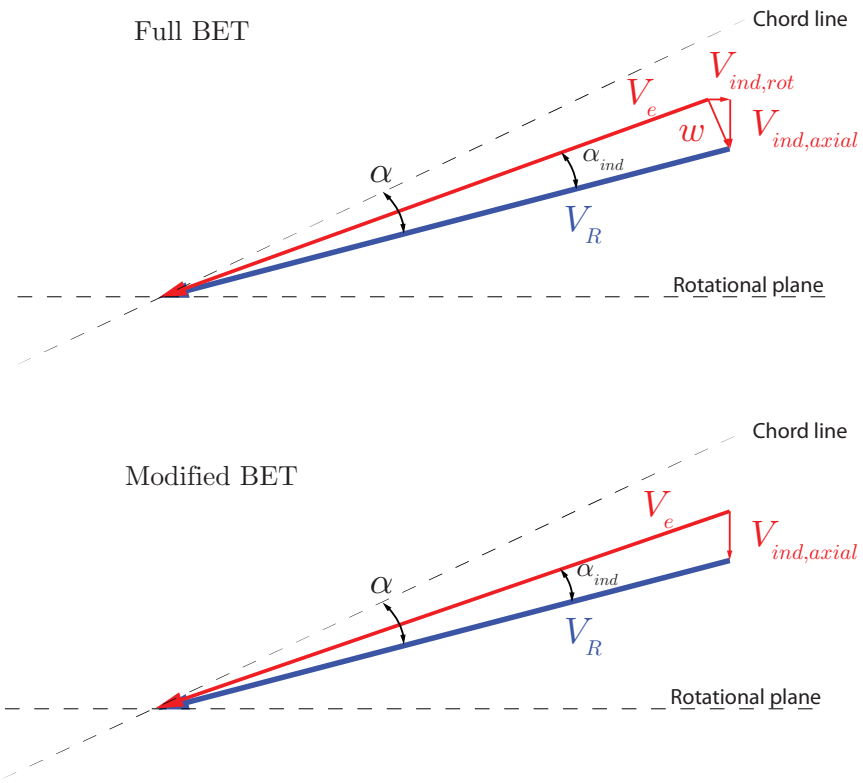

Figure 2.10: Modified flow case, neglecting induced velocities in the rotational direction

The combined BEM theory can be applied in aerodynamic analysis using the following general iterative scheme.

1. Guess an increase in velocity, u', at the propeller disc
2. Perform BET for the propeller blades and find the total thrust and torque
3. Calculate thrust and torque using Actuator Disc Theory
4. Recalculate u' from ADT results
5. Compare against initial guess of u'
6. Update guess of velocity increase
7. Iterate until convergence is reached

2.4 Airfoil characteristics

Early on in propeller research, it was clear that the high relative speed of the propeller posed serious problems when flying fast. This manifested as large losses in lift force and increase in drag and was termed the "compressibility burble" [17]. The problem originated in the desire to push airplanes faster and since the propeller moves a lot faster relative to the airspeed there was a distinct limit in speed for propeller driven aircrafts [18]. Structural considerations also made this effect accentuated at the root sections of the blades, where the blades generally are thicker.

The "compressibility burble" problem arises when the local speed reaches supersonic magnitudes over the airfoil surface, forming a supersonic pocket on the suction side of the airfoil. While the free stream velocity is subsonic, portions of the propeller or wing can exhibit supersonic flows [10]. This means that for a given flight speed V_∞ which yields a flight Mach number, there is a critical Mach number were the local speed over the airfoil reaches Mach 1 due to to low pressure [10]. Most airfoils used for propellers in the 1920's and 30's had large negative pressure distributions on the suction side of the airfoil, forming suction peaks near the leading edge [18], which promoted the forming of supersonic pockets. An idea to counter this was to decrease the induced velocities close to the leading edge by moving the center of minimum pressure or *suction peak* further aft along the chord. This idea gave birth to the NACA 16-family [18].

2.4.1 NACA 16-airfoils

NACA 16-airfoils are designed for high speed applications, with the goal to delay the forming of the supersonic pocket while still maintaining a good lift/drag ratio [18]. Unlike its predecessors, the four- and five-digit NACA series, the shape of the airfoil is derived from airfoil theory rather than analytical expressions based on experiments [19]. The airfoil family is described using the following notation:

NACA 16-XYY

where the first number is a series designation. The second number indicated the location of minimum pressure for a symmetric section at zero lift, in tenths of the chord. The 'X' designated the amount of camber expressed in terms of the design lift coefficient, in tenths. The last letters,'YY', give the profile thickness in percentage of the chord [19].

Due to the extensive research carried out around this particular airfoil family, e.g. [18] [20] [21] there is a lot of data available. Since the scope is not directed towards optimizing the performance of the local airfoil sections, the NACA 16-family is used throughout the work. Figure 2.11 shows a NACA 16-409 airfoil, which from the notation has a design lift coefficient of 0.4 and a maximum thickness of 9% of the chord.

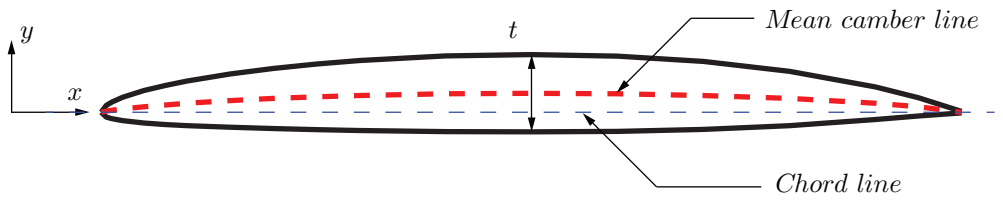

Figure 2.11: The anatomy of a NACA 16-409 aifoil

2.5 Mechanical theory

Herein, the theory relevant for the structural assessment of the box-blades are presented. Firstly, the forces acting on a propeller blade in flight are identified. Thereafter, the elementary methods for structural analysis of the blades are presented.

2.5.1 Forces acting on propeller blades

To get an idea on the structural stress in the box-blade at a given flow condition, the forces acting on a propeller blade must first be identified. The forces acting on a propeller blade in flight is divided into three categories. The forces are shown in Figure 2.12.

1. Inertial forces (centrifugal forces) on the blades
2. Aerodynamic forces (composed of thrust bending forces, torque bending forces, aerodynamic twisting moments and inertial twisting moments)
3. Vibrational forces and resonance

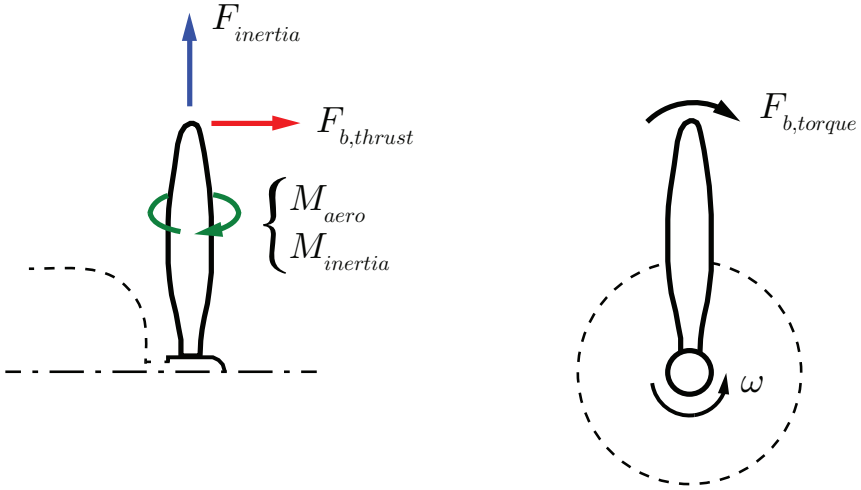

Figure 2.12: Some of the forces acting on a propeller blade

The greatest force out of these categories are inarguable the inertial forces, trying to pull the propeller blades off the hub. It is not uncommon that these forces are several magnitudes higher than the actual weight of the blade, which is easily realized from the equation for inertial force using Newtons second law in a rotating frame of reference

$$F_{inertia} = ma = m\left(\omega^2 r\right) \tag{2.22}$$

or in vector notation

$$\mathbf{F}_{inertia} = m\mathbf{a} = m\left[\omega \times \mathbf{V}\right] = m\left[\omega \times (\omega \times \mathbf{r})\right]$$

From Equation 2.22 it is clear that if the rotational speed is doubled, the inertial force is quadrupled at a given radius. A good but rather disturbing analogy can be made with a fan blade of the Airbus A380. At take-off, the inertial forces acting on *one* fan blade is equivalent to the weight of a main-line locomotive which amounts to a force around 1000 kN [22].

The aerodynamic forces are much smaller in magnitude compared to the inertial forces, and may also works counteracting to some degree [23]. The thrust bending moment bends the propeller blades in the direction of flight and somewhat opposes the inertial force pulling the blades apart. The inertial twisting moments acts to decrease the blade angles and opposes the aerodynamic twisting moments, which increases the blade angles. The aerodynamic forces are also closely related to the third category, the vibrational forces and resonance in the structure of the blades.

Since vibrations and resonance are related to the dynamic behavior of the blade, the third category of forces is not investigated further in this thesis. In addition, the only forces taken into account in the mechanical analysis are the inertial forces, with the motivation that they a lot larger in magnitude compared to the aerodynamic forces [23].

2.5.2 Simple modeling of box-blade geometry

The box-bladed propeller has a quite complex geometry; the box-blade might be arced with both forward- and backward sweep and furthermore rotated and twisted in different directions.
A first approach to define the blade mechanically is using a simple case that might resemble the box-bladed shape and has the properties desirable for the mechanical requirements of the blade. Two proposed simple models; a diamond/triangular and boxplane configuration is shown in Figure 2.13.

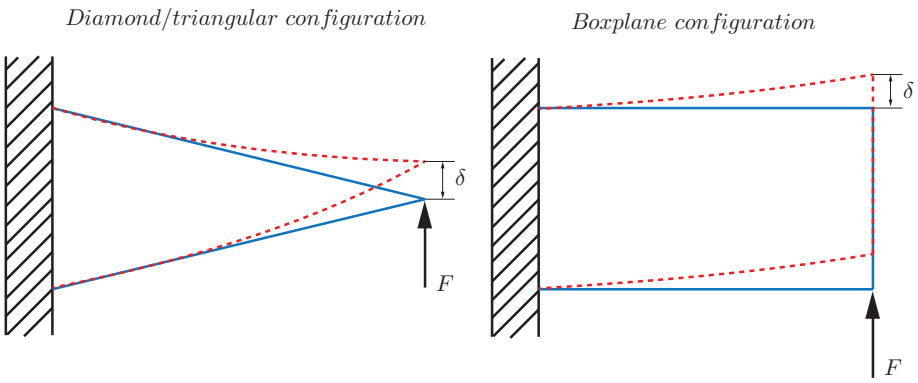

Figure 2.13: Simplified beam models suggestions for the box-blade

From previously performed structural assessments [3], a suggestion is to combine the two models and adapt the shape with intentions to bring the bending moments to a minimum. One such approach is by using a *catenary curve*, also called chainette.

The catenary curve

Imagine a chain suspended between two poles. If the chain is longer than the distance between the poles it will bow down in a particular shape, which can be described by a catenary curve. This arced shape is often used in architecture and structural engineering for arched vaults, bridges and portals.

Mathematically, the catenary can be described by a hyperbolic function in Cartesian space

$$y = a \cosh\left(\frac{x}{a}\right) \tag{2.23}$$

where the coefficient a determines the curvature of the catenary curve.

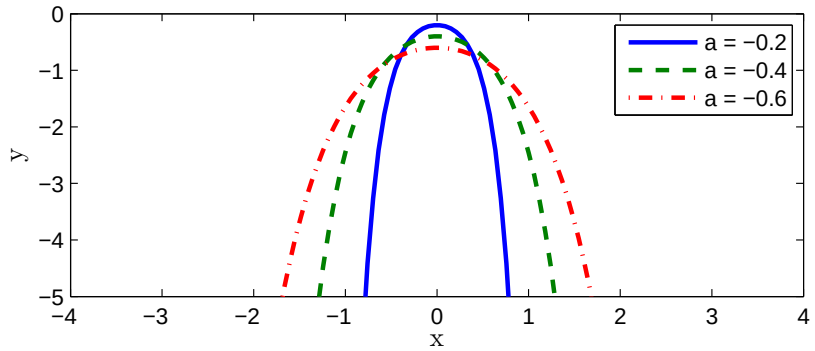

Figure 2.14: Using Equation 2.23 with different values on a to create a number of inverted catenary arcs

The inverted catenary arc shape is well suited for the box-bladed concept, since it admits a smooth transition at the tip of the two fused single blades. In this way, sharp corners are avoided to a higher degree than the original design approaches and stress concentrations due to abrupt changes in geometry are minimized. Manufacturability is a different question but not treated to further extent in this work.

2.5.3 Bending of curved beams

From the description in Section 2.5.2 it is clear that the proposed beam shape is nothing like any elementary cases in structural mechanics. One must resort to generalized three-dimensional beam theory and elementary equations to solve the forces, moments and stresses acting on the blade. There are some research available on this topic, e.g. [24] [25] and [26]. However, to investigate this regarding the scope of this thesis would not be realistic and has been left as a future recommendation.

The stresses in the beams have instead been assessed using elementary beam theory, only taking the shear force into account. From simple beam theory according to Euler-Bernoulli, the forces acting on a beam can be described by the a cross-sectional approach used

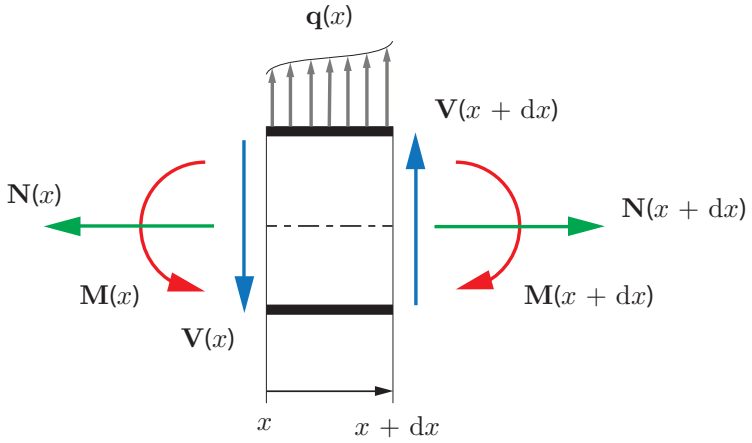

Figure 2.15: Cross-sectional forces and moments of a beam section using classic sign convention

3

Method

3.1 Box-blade geometry design method

This section describes the development of the box-blade geometry and how it is generated. The main parameters shaping the blade orientation in cartesian space is described. Furthermore, the generation of the actual aerodynamic blade shape is outlined

3.1.1 The box-blade stacking line

Traditionally when designing propeller blades or blades for turbo machinery applications, the geometry of a blade is defined by a line starting from the blade root to the blade tip called a stacking line. This allows for an easy representation of the blade as a function of radius. With the box-blade concept however, this might prove to be problematic since there will be multiple points at a given radius excluding the local maximum point at the blade tip. Applying equations may then prove troublesome since there could be two solutions for any given radial blade position. Instead of describing the stacking line coordinates based on the radius, an independent parameter is introduced. This parameter will henceforth be called the *stacking line parameter* and is abbreviated s

The stacking line parameter is constructed in such a way that the two separate blades that make up the final box-blade loop is easily distinguished from one another. For simplicity, the parameter is given the value 1 and -1 at the two blade roots and the value 0 at the tip. This allows for an easy representation of the stacking line from one blade root, through the tip to the second blade root with a discrete number of points varying linearly from -1 to 1. A principal sketch of the stacking line parameter is shown in Figure 3.1

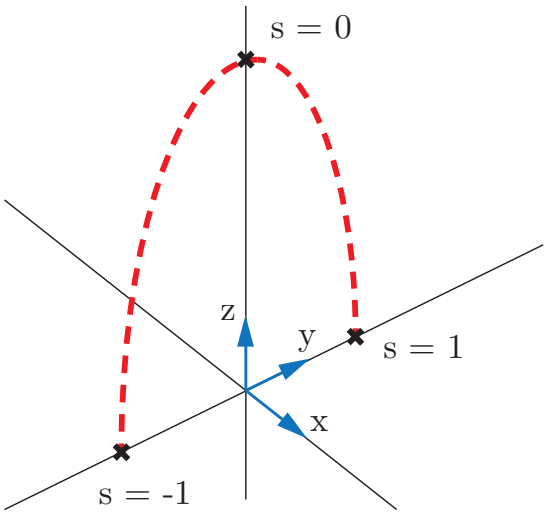

Figure 3.1: Simple parabola-shaped stacking line sketch with the two blade roots and blade tip marked

To construct the stacking line geometry in three-dimensional Cartesian space, the stacking line is described as a set of polynomial functions dependent on the stacking line parameter, s. By introducing higher order terms and varying coefficients, the stacking line can be manipulated to the desire shape. Requirements on the shape of the stacking line shape might also be defined by angles and geometrical constraints, but since the process of generating the geometry is generic at this point the polynomial approach is good for easy changes in stacking line shape. An arbitrary point on the stacking line is defined by the vector

$$\mathbf{X}_{stack}(s) = \begin{bmatrix} x'(s) & y'(s) & z'(s) \end{bmatrix} \tag{3.1}$$

with the coordinates $x'(s)$, $y('s)$ and $z'(s)$ defined by polynomial functions. The global coordinate system is defined so that positive x generally is in the direction of flight and the y- and z-directions make up the coordinates in a rotational plane along the direction of flight. This *global* coordinate system is used throughout the work. An example of the polynomial functions used to generate the preliminary geometry of the stacking line is

$$x'(s) = l_{sweep} \left[c_1(1-s^2) + c_2(1-s^2)^2 \right] \tag{3.2}$$

$$y'(s) = \frac{1}{2} l_{root}(s - d_1 s^3)/(1-d_1) \tag{3.3}$$

$$z'(s) = R_{hub} + (R_{tip} - R_{hub})(1-s^2) \tag{3.4}$$

where l_{root} is the blade root baseline spacing, l_{sweep} is a sweep parameter controlling sweep in the x-direction, R_{hub} and R_{tip} are the hub at tip radiuses. c_i and d_i are constants.

The polynomial function in the x-direction will govern the blade sweep in the axial direction, which through manipulation can be set as both forwards and backwards sweep. The y-polynomial controls the curvature of the blade arc in the rotational plane, analogous with the catenary curve described in Section 2.5.2. The z-polynomial will set the radius at each stacking line point, when initially building the stacking line symmetrically around the z-axis. Combining the y and z-coordinate will yield the radial coordinate w.r.t. the center of rotation in the global coordinate system.

3.1.2 Modifying the initial stacking line

With the stacking line defined in the global coordinate system, with a certain curvature and sweep, one might desire to modify it to allow for a geometry that is better in terms of aerodynamical and structural considerations. The whole stacking line might be rotated around the global z-axis, thus providing a more suitable angle when stacking the profiles with respect to the relative inflow. The most simple way to do this is rotating the whole stacking line about the global z-axis. This is easily done using a rotational matrix

$$\mathbf{X}_{stack,mod} = \mathbf{R}_z \, \mathbf{X}_{stack} = \begin{bmatrix} \cos\epsilon & \sin\epsilon & 0 \\ -\sin\epsilon & \cos\epsilon & 0 \\ 0 & 0 & 1 \end{bmatrix} \begin{bmatrix} x' \\ y' \\ z' \end{bmatrix}$$

where ϵ is the *axial displacement angle*. Local rotations might also be applied, but for a first stacking line approximate geometry the same rotation is applied to every point. The axis of rotation might also be redefined introducing a warping effect in the stacking line (rotating at different degrees along the line). Figure 3.2 shows a sketch of the effect of an axial displacement being applied to the stacking line.

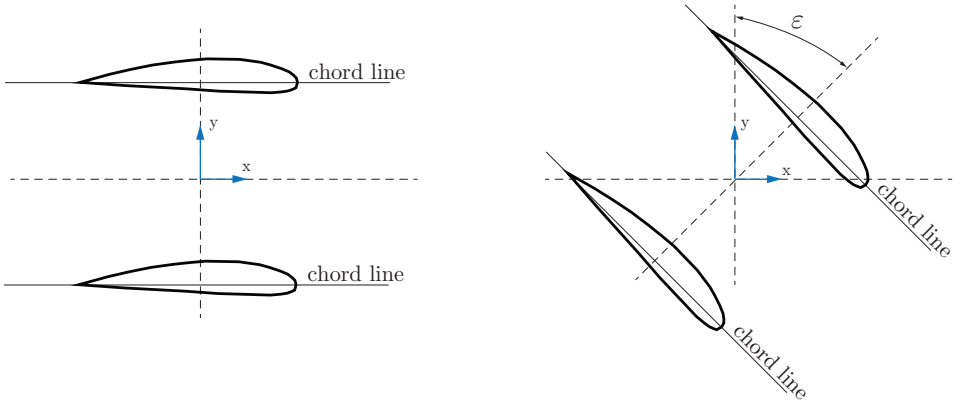

Figure 3.2: Sketch of an axial displacement of 45 degrees

Another parameter to consider is defined in previous works as the *chord displacement angle* [1], given the notation ζ. In this report, the chord displacement angle refers to the

"shearing" of the stacking line, given by the chord displacement in a certain slice of the blade. One such slice is illustrated in Figure 3.3. The idea originates from the biplanes of the early 20th century, which utilized two wings. The wings on the biplanes were not always positioned in line, but the lower or upper wing could be mounted ahead or behind the other in the direction of flight. This displacement in the fore and aft direction is called *stagger* when talking about biplane wing and apparently has little or no effect on the drag [27]. The main reason for stagger was instead to provide unobscured vision for the pilot.

When the leading edge points of the two blade roots and their respective chord lines are perpendicular, the chord displacement angle is zero. When the leading blade in the direction of flight and rotational direction is ahead of the trailing blade, ζ is positive and negative ζ is vice versa. Varying ζ might be favorable when considering the platform size of the actual propeller blades mounted on an engine and constraints regarding the mechanical pitching of the blades can be controlled [1]. It may also be a way to improve the box blade aerodynamics. Since the scope of this thesis does not cover platform aspects, ζ has not been studied in more detail. It is nonetheless implemented in the geometry generation code for future studies

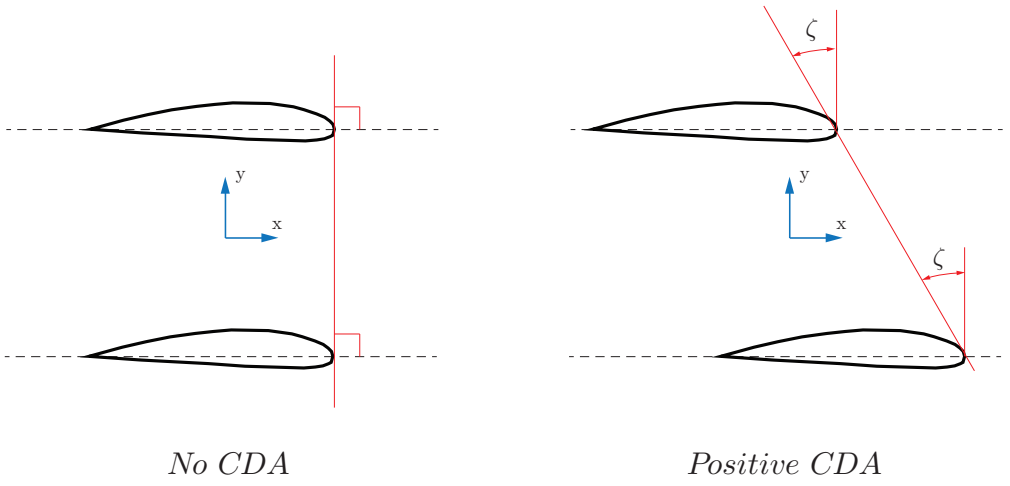

Figure 3.3: Sketch showing the idea of the chord displacement angle

Furthermore, the vertical distance between the two wings has a significant effect on the drag [27]. The distance is for biplanes termed *gap* and is limited by the structural considerations regarding the wing support structure. If the gap is narrow, the overall drag is increased due to interference effects between the wings [27]. The structural issues associated with the gap on the box-blades, defined by the distance between the two separate blades, l_{root} , is of lesser importance than for a wing because a propeller does not have the same structural construction as a wing (wing beams connecting to the fuselage, overall

weight etc.). Nonetheless, the interference effect between the two blades is not negligible and will as in the case of biplanes most likely increase the overall drag of the box-blade, especially close to the blade tip. Because of the basic aerodynamic methods used, the effects of interference between the two box-blade parts is not investigated to further extent.

For the preliminary design geometry, the axial displacement ϵ is set to 45° and the chord displacement angle ζ to 0°. Using the polynomial functions from Equations 3.2 through 3.4, the preliminary stacking line with axial displacement angle applied is displayed in Figure 3.4

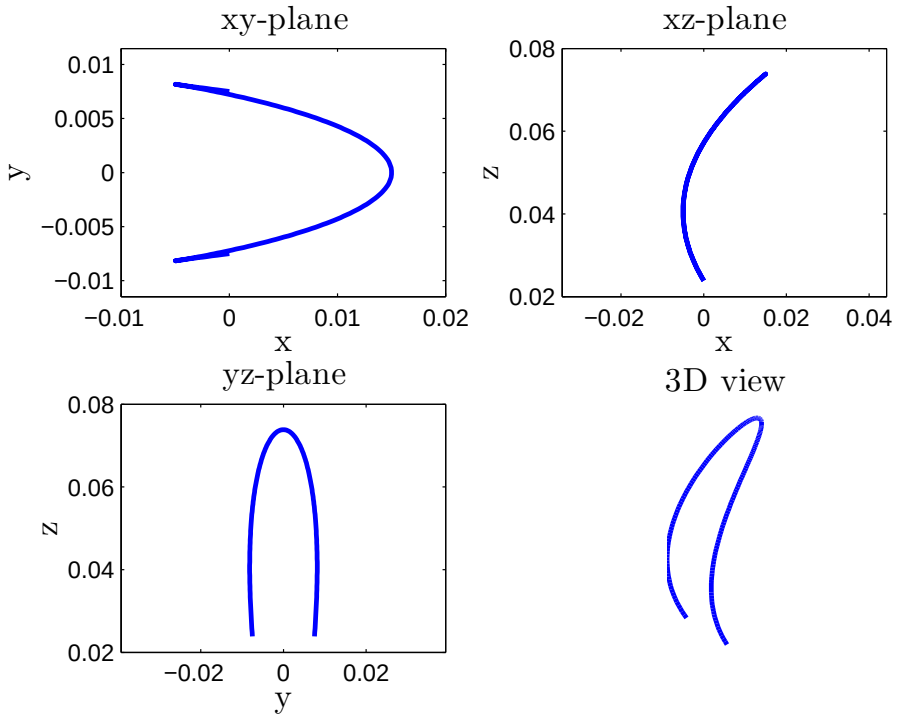

Figure 3.4: Visual representation of the stacking line (before axial displacement is applied)

3.1.3 Reference geometry generation from ADP

Initially, the blade is designed with respect to the Aerodynamic Design Point, henceforth abbreviated ADP. In order to design the blades from the flow conditions, the approach taken is by defining local velocity vectors and relating them to the stacking line. From this, the plane on which the airfoil profiles are laid out can be constructed. Assuming a stacking line fixed in space described by the stacking line parameter, the unit tangent vector at each point of the stacking line can be obtained. Using numerical differentiation (applying a central difference scheme) on the stacking line coordinate matrix, the unit tangent vector at each point becomes

$$\hat{\mathbf{e}}_t = \frac{d\mathbf{X}_{stack}}{ds} \Big/ \left| \frac{d\mathbf{X}_{stack}}{ds} \right| \tag{3.5}$$

By defining a relative inflow velocity at the propeller blades; the axial inflow being the flight speed of the propeller and the angular velocity of the blades the relative velocity vector at each stacking line point can be obtained through vector summation. Defining the normalized unit vector of the relative velocity at each point along the stacking line

$$\hat{\mathbf{e}}_v = \frac{\mathbf{v}_R}{|\mathbf{v}_R|} \tag{3.6}$$

Using the unit vectors in Equations 3.5 and 3.6, the local plane onto which each profile will be stacked can be defined. It is desirable to define the local profile plane to have a normal which is pointing in the tangential direction of the stacking line, but not necessarily in the tangential direction. Furthermore, the plane should extend in the direction of the relative velocity. This will provide an easy control of the local profile line-up and admit control of airfoil parameters such as the angle of attack. To express the unit normal vector to the local profile plane $\hat{\mathbf{e}}_{pn}$ in terms of the vectors in Equations 3.5 and 3.6 the unit tangent vector is projected on a plane perpendicular to the relative velocity vector, like so

$$\hat{\mathbf{e}}_{pn} = \frac{\hat{\mathbf{e}}_t - \hat{\mathbf{e}}_v \left(\hat{\mathbf{e}}_t \cdot \hat{\mathbf{e}}_v\right)}{\left|\hat{\mathbf{e}}_t - \hat{\mathbf{e}}_v \left(\hat{\mathbf{e}}_t \cdot \hat{\mathbf{e}}_v\right)\right|} \tag{3.7}$$

Defining the vectors from Equations 3.5, 3.6 and 3.7 gives the tools to define the coordinates for each local airfoil profiles along the stacking line. The relative velocity vector is collinear with the chord vector of a profile at zero angle of attack and will make the base of the abscissa (local x-coordinate, see Figure 2.11) of the profile. With the normal to the local propeller plane defined, the vector representing the ordinate (local y-coordinate) of the airfoil profile can be defined as the cross product of the relative velocity and local profile normal vectors ($\hat{\mathbf{e}}_{pn} \times \hat{\mathbf{e}}_v$). Figure 3.5 depicts the tangent vector, the relative velocity vector, the local profile plane normal and the cross product of the two latter vectors for a number of points along the stacking line, the backbone of the local profile plane.

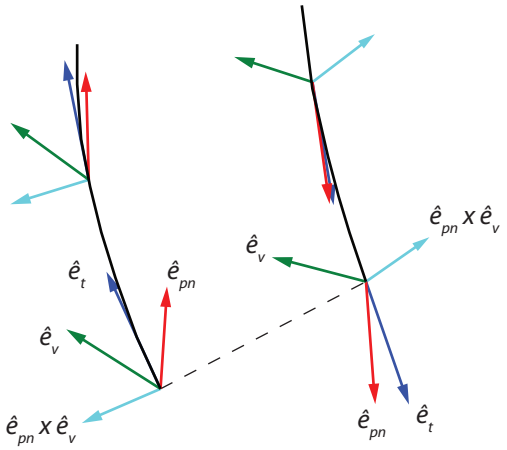

Figure 3.5: Tangent, relative velocity, local profile plane normal and thickness vectors for a set of points close to the blade roots

Before the profiles can be stacked, the coordinates for the leading edge and trailing edge are calculated. The coordinates for the leading and trailing edge point is obtained by starting from a given stacking line point and using the unit vectors and the specified chord length at the particular point. The stacking line is normally situated at a fraction of the chord length from the leading edge, defined by μ. The value of μ for airplane wings is often set to 0.25 which is the aerodynamic center of the airfoil, where the moments from aerodynamic forces are independent of the angle of attack [9]. However, since the aerodynamic forces affecting the airfoil is of less interest for a fast propeller, the value is set to 0.5 for reasons of symmetry and mid chord sweep theory. The leading edge and trailing edge points may now be expressed as a function of the vectors defined in Equations 3.6 and 3.7 with a desired angle of attack α with respect to the relative velocity vector

$$\mathbf{X}_{lead} = \mathbf{X}_{stack} + \mu \, \mathrm{c} \left[\cos(\alpha) \, \hat{\mathbf{e}}_v + \sin(\alpha) \, (\hat{\mathbf{e}}_{pn} \times \hat{\mathbf{e}}_v) \right] \tag{3.8}$$

$$\mathbf{X}_{trail} = \mathbf{X}_{stack} + (1 - \mu) \, \mathrm{c} \left[\cos(\alpha) \, \hat{\mathbf{e}}_v + \sin(\alpha) \, (\hat{\mathbf{e}}_{pn} \times \hat{\mathbf{e}}_v) \right] \tag{3.9}$$

with c being the chord length of the local airfoil profile. For an arbitrary flow case, the leading edge could be described by an independent stacking line parameter, different from s. Naming this parameter u, Equation 3.8 may be rewritten as

$$\mathbf{X}_{lead}(u) = \mathbf{X}_{stack}(s) + p \, \hat{\mathbf{e}}_v + q \, (\hat{\mathbf{e}}_{pn} \times \hat{\mathbf{e}}_v) \tag{3.10}$$

with u,p and q being unknown parameters. From this, the leading edge point can be determined from a general flow field. Equation 3.10 gives three scalar equations for three unknown variables, a solvable system. This is however a tedious process when investigating a lot of different flow cases and a simplified method might be desirable for

easy off-design analysis. One approach is fixing the geometry with respect to the design flow field, defined by the ADP. This implies that

$$\mathbf{X}_{lead}(u) \equiv \mathbf{X}_{lead}(s)$$

This means that the leading edge points (and analogously the trailing edge points) can be generated once using the stacking line coordinates at the aerodynamic design point. In reality, this is consistent with a propeller having a *fixed pitch* meaning that the blade geometry is fixed in space and the propeller hub has no pitching mechanism. The helix angles will then only be dependent on the flow field. Since the geometry constructed for the rig tests will not have any pitch mechanism [2], the assumption is valid since the propeller will be designed and tested out at a predefined ADP. To find angles of attack at off-design points, Equation 3.8 may be rewritten

$$\mathbf{X}_{lead}(s) - \mathbf{X}_{stack}(s) = \mu \, \mathrm{c} \left[\cos(\alpha) \, \hat{\mathbf{e}}_v + \sin(\alpha) \, (\hat{\mathbf{e}}_{pn} \times \hat{\mathbf{e}}_v)\right]$$

Multiplying by $(\hat{\mathbf{e}}_{pn} \times \hat{\mathbf{e}}_v)$

$$(\mathbf{X}_{lead} - \mathbf{X}_{stack}(s)) \cdot (\hat{\mathbf{e}}_{pn} \times \hat{\mathbf{e}}_v) = (\mu \, \mathrm{c}) \sin(\alpha)$$

and dividing by $\mu \, \mathrm{c} = |\mathbf{X}_{lead} - \mathbf{X}_{stack}|$ yields:

$$\sin(\alpha) = \frac{(\mathbf{X}_{lead} - \mathbf{X}_{stack}) \cdot (\hat{\mathbf{e}}_{pn} \times \hat{\mathbf{e}}_v)}{|\mathbf{X}_{lead} - \mathbf{X}_{stack}|} \tag{3.11}$$

which will give the angle of attack, α, at off-design points. In the same manner, the blade angles β can be defined. The blade angle for a given box-blade section is calculated by projecting the chord on plane which is normal to the radial vector extending from the center of rotation

$$\tan(\beta) = \frac{x(\mathbf{X}_{lead}) - x(\mathbf{X}_{stack})}{r(\mathbf{X}_{stack}) \left[\arcsin\left(\frac{y(\mathbf{X}_{lead})}{r(\mathbf{X}_{stack})}\right) - \arcsin\left(\frac{y(\mathbf{X}_{stack})}{r(\mathbf{X}_{stack})}\right)\right]} \tag{3.12}$$

At the tip, the blades might be set at an angle relative to the horizontal line tilting the blades inwards or outwards in the direction of flight. This angle has been named the *convergence angle* γ and is defined by the angle relative to the horizontal axis, in a plane which passes through the center of rotation and the given stacking line point

$$\tan(\gamma) = \frac{r(\mathbf{X}_{lead}) - r(\mathbf{X}_{stack})}{x(\mathbf{X}_{lead}) - x(\mathbf{X}_{stack})} \tag{3.13}$$

Note that the angles are dependent on the flow field. As stated in Equation 3.10, it is possible to define the angles independent of the flow field. This will however require solving of the system of equations that can create problems since there might not be a unique solution at each point, with the stacking line being curved. With the ADP set for the preliminary geometrical design, the leading and trailing edge points are computed from Equations 3.8 and 3.9. The chord lines at each stacking line point are now defined.

Shown in Figure 3.6 are the chord lines of the blade roots

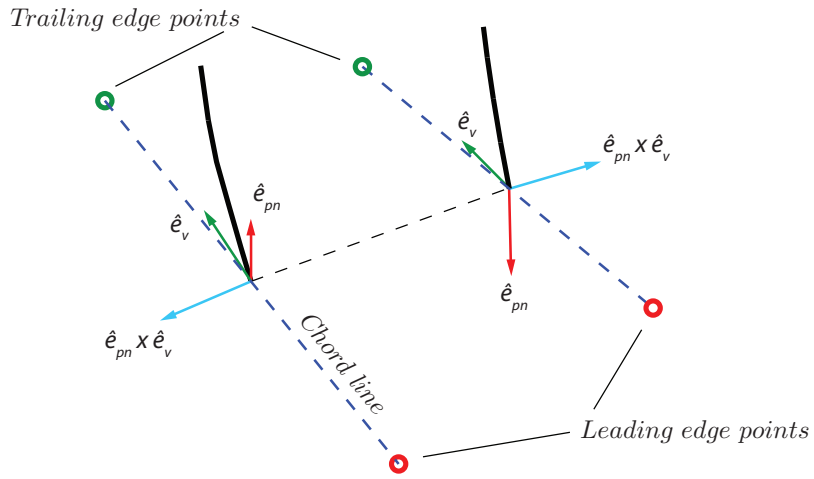

Figure 3.6: Chord lines for the root stacking line points, defined by the computed leading edge and trailing edge points. Note that the chord lines are laid out with an angle of attack with respect to the relative velocity

With a local profile plane defined and reference points for the leading and trailing edges at each stacking line point, the profiles can be plotted along the stacking line. To accomplish this, a subfunction has been created which takes geometrical input data in the form of chord length, maximum thickness and design lift coefficient as defined in Section 2.4 and scales the profile accordingly. Knowing the position of the leading edge points, a vector can be constructed which is directed along the chord line

$$\hat{\mathbf{e}}_{chord} = \frac{\mathbf{X}_{lead}(s) - \mathbf{X}_{stack}(s)}{|\mathbf{X}_{lead}(s) - \mathbf{X}_{stack}(s)|} \tag{3.14}$$

With the local profile plane normal already defined from Equation 3.7, the cross product of the chord vector and local profile normal vector will define the thickness of the airfoil, perpendicular to the chord line.

$$\hat{\mathbf{e}}_{thick} = \hat{\mathbf{e}}_{pn} \times \hat{\mathbf{e}}_{chord} \tag{3.15}$$

This distinguishes the local airfoil vectors $\hat{\mathbf{e}}_{chord}$ and $\hat{\mathbf{e}}_{thick}$ from the local flow vectors $\hat{\mathbf{e}}_v$ and $\hat{\mathbf{e}}_{pn} \times \hat{\mathbf{e}}_v$. The profiles are now rotated about the local stacking line point using the local airfoil vectors. The rotation aligns each profiles with respect to the chord line and is accomplished using a simple rotational matrix

$$\mathbf{X}_{coord,local} = \mathbf{R}_{profile}\, \mathbf{X}_{coord} = \begin{bmatrix} \hat{\mathbf{e}}_{chord}(s,1) & \hat{\mathbf{e}}_{chord}(s,2) & \hat{\mathbf{e}}_{chord}(s,3) \\ \hat{\mathbf{e}}_{thick}(s,1) & \hat{\mathbf{e}}_{thick}(s,2) & \hat{\mathbf{e}}_{thick}(s,3) \\ \hat{\mathbf{e}}_{pn}(s,1) & \hat{\mathbf{e}}_{pn}(s,2) & \hat{\mathbf{e}}_{pn}(s,3) \end{bmatrix} \begin{bmatrix} x_{coord} \\ y_{coord} \\ z_{coord} \end{bmatrix}$$

where $\mathbf{X}_{coord}$ are local airfoil coordinates scaled with thickness, chord and camber and $\mathbf{X}_{coord,local}$ are the local coordinates in the local profile plane at each stacking line point. Figure 3.7 shows the two root profiles laid out with respect to the local airfoil vectors.

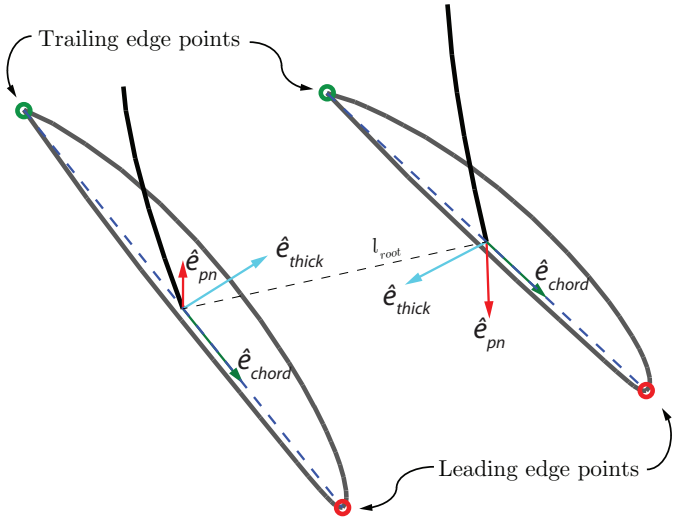

Figure 3.7: Profiles stacked at the blade roots

Repeating this for the entire stacking line will yield the final geometry of the box blade. Since the blade profiles are constructed using the relative flow field, the leading and trailing edge points may be placed outside the actual hub. This may generate problems at the blade roots if the stacking line is set to start at the desired hub radius. In fact, there might be a gap between the hub surface and the root profile surface. To counter this, the stacking line is set to start at a fictive hub radius lower than the actual hub radius while still maintaining the parameter values $s = -1$ and $s = 1$ at the blade roots. The excess blade material is then easily cut off when importing the profiles into a CAD software. Figure 3.8a shows 25 profiles stacked along the stacking line and from Figure 3.8b the blade is shown in a solid model state, resembling the final 3D model

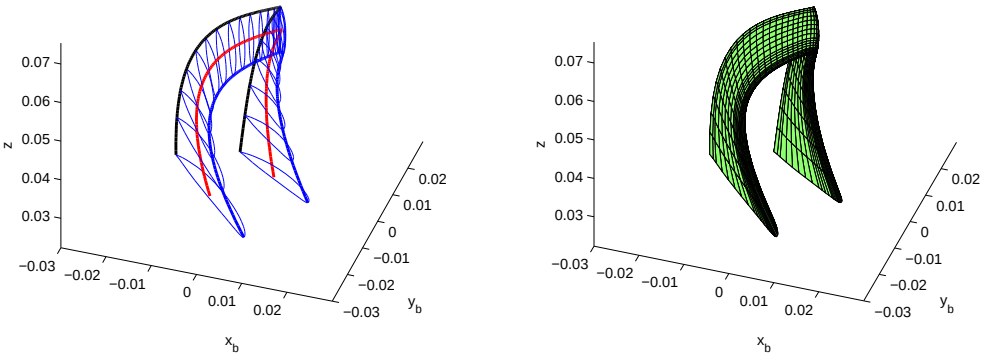

(a) Stacked profiles **(b)** Solid blade

Figure 3.8: Stacked profiles to the left, solid representation to the right

The profiles are easily exported as text files and read into any CAD software, where the profiles can be turned into a solid model for manufacturing. In this thesis, the profiles are exported to Autodesk Inventor® and made into a solid model using a loft command[1]. When imported, the profile points are turned into a continuous line using a spline approximation built into the software. The three-dimensional shape is also interpolated between profiles when using the loft command which means that the number of profiles that need to be imported are lowered. Special care has to be taken when the curvature is large, e.g. at the blade tip meaning that the number of imported profiles has to be somewhat denser here in order to capture the shape correctly. It was found that around 25 profiles along the stacking line yields a satisfactory geometry.

The blade is fitted with a hub that has been constructed to fit the propeller test rig, see [2], and the single imported blade is copied in a rotational pattern to form the first test propeller prototype. The blades are manufactured using rapid prototyping technology.

3.2 Reference propeller aerodynamic analysis method

The box-bladed propeller will be designed at a specific aerodynamic design point as mentioned in Section 3.1.3. The ADP is in general defined by the operating point of the propeller which dominates the flight cycle, being *cruise conditions* in most cases. Because of the model scale and restrictions on equipment and material, cruise speed is not included in the scope of this thesis work. The ADP is instead set to a condition matching take-off, also called end-of-runway (EOR). This will give propeller tip speeds

[1] Extrudes a solid model using several shapes, into one continuous object

close to 200 m/s corresponding to Mach 0.6.

At the ADP, the propeller is designed to perform with maximum efficiency. To assess the performance of the propeller at conditions different from the ADP, off-design analysis is performed. As mentioned in Section 3.1.3 the propeller geometry is designed with a fixed pitch which makes it interesting to investigate how the propeller performs when the flow conditions are changed. With a pitchable propeller, the blades can be rotated to better meet the relative flow giving a better overall efficiency over the entire operating range. For the fixed pitch propeller, the blade geometry is fixed and the propeller speed (yielding different blade angles) will constitute the performance at off-design points.

Since no test data or numerical data for the performance of box-bladed propellers are available, the aerodynamic analysis was developed with the help of reference model propeller data. The method development process will be described in this section.

3.2.1 Method development using conventional propeller and test data

At the University of Illinois in Urbana-Champaign, professor Michael Selig at the Department of Aerospace Engineering has performed extensive research on small scale propellers. The research is particularly interesting with the increase in applications invloving model-sized propellers designed for miniature UAVs[2]. An extensive database of test data from wind tunnel measurements at low Reynolds numbers are available [28]. The experimental procedure is thoroughly described by J. Brandt et. al, see [29].

For the aerodynamic analysis method development, a propeller with a simple and generic geometry was chosen from the propeller database [28]. The Graupner Super Nylon 11×6 was adopted as the basis for the method development. It has a diameter of 11 inches ≈ 280 mm and a pitch of 6 inches ≈ 153 mm, meaning that for one turn of the propeller advances 153 mm. The propeller planform is fairly symmetrical which is desirable in order to diminish geometrical effects of bent propeller tips etc. The planform is depicted in Figure 3.9.

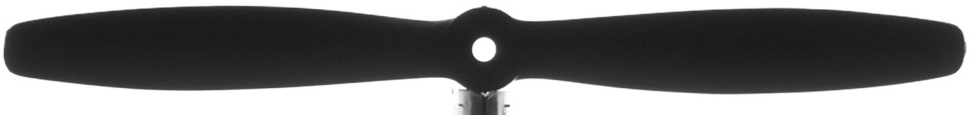

Figure 3.9: Planform of the Graupner Super Nylon 11x6 propeller used for method development (Adapted from [28])

[2]Unmanned Aerial Vehicle

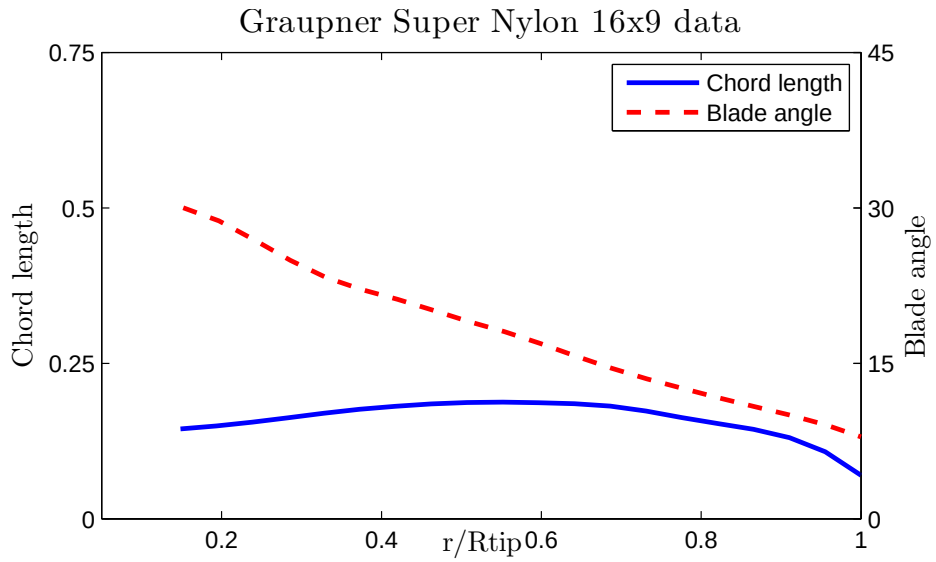

Figure 3.10: Chord and blade angle with respect to radius [28]

From the database, the chord and blade angles of the propeller are plotted with respect to radius, see Figure 3.10. This provides the geometrical input for the analysis code. The results of the wind tunnel experiments are plotted using the non-dimensional quantities defined in Section 2.2 and should hence be evaluated in the analysis code. The numerical procedure of determining the performance data is outlined in the flowchart in Figure 3.11. The method utilizes the BET theory described in Section 2.3.1 with the modified flow case described in Section 2.3.3 together with Actuator Disc Theory described in Section 2.3.2.

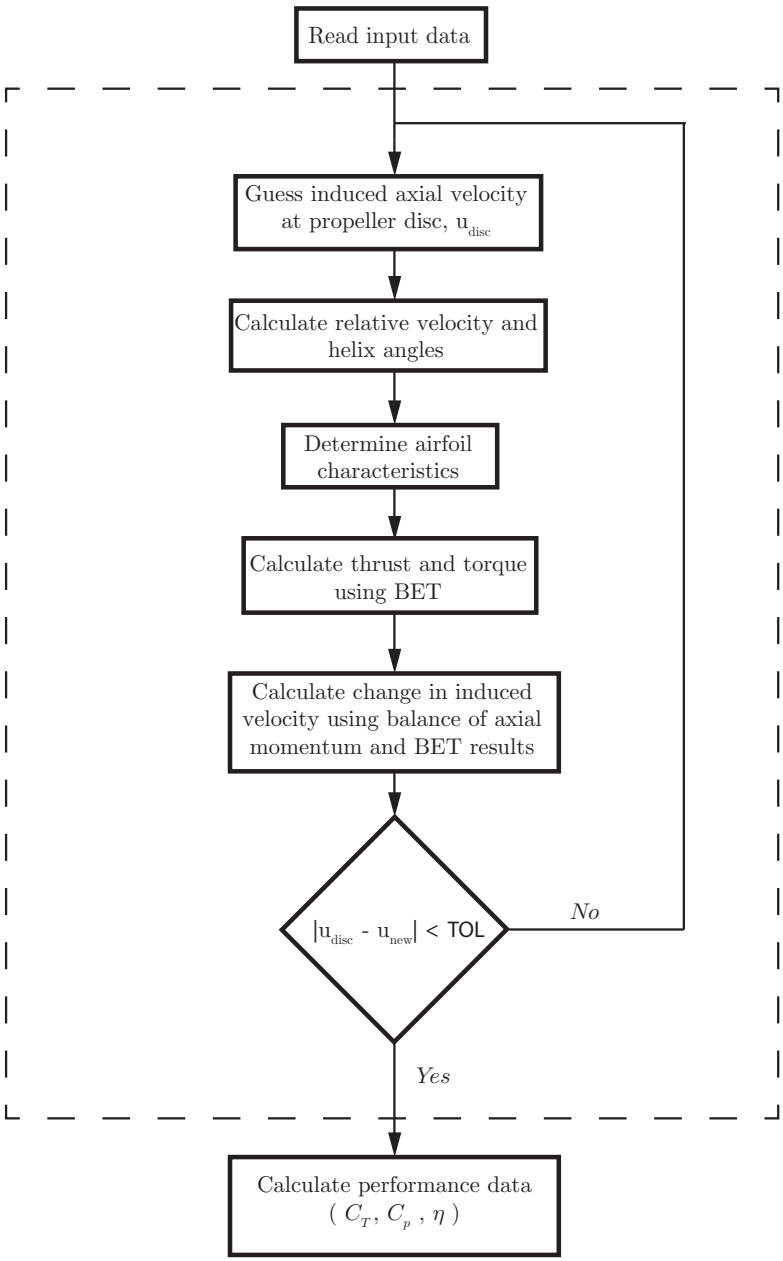

Figure 3.11: A flowchart outlining the calculation procedure of the aerodynamic analysis of the reference propeller

3.2.2 Determining the airfoil characteristics

As mentioned in Section 2.4 there is a lot of data available from experiments for the NACA 16-family. The appendix of a report by Sand et. al [21] has airfoil characteristics (c_l and c_d) for NACA 16-airfoils ranging from thicknesses of 4 to 21 percent and design

lift coefficients from 0 to 0.6. These thicknesses and design lift coefficients are thought to be adequate for the design of the box-bladed propeller investigated in this thesis. Furthermore, the data provides measurements for Mach numbers ranging from 0.3 to 1.6 which allows for analysis in the transonic range.

The airfoil sections of the Graupner Super Nylon propeller are most likely not NACA 16 but as a first approximation, the airfoils are taken to be NACA $16-2YY$ which means a design constant lift coefficient of 0.2 over the whole blade radius. In order to use the data from the diagrams in [21], the data has been digitized and read into Matlab®. The diagrams from the report and the digitized version is shown in Figure 3.12.

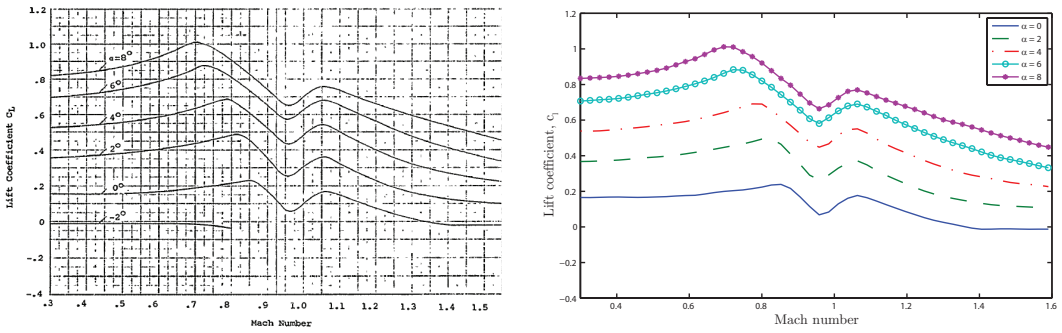

Figure 3.12: Original report diagrams of c_l (adapted from [21]) and the digitized counterpart used in the subroutine

A subroutine then calculates the lift and drag coefficients from input data. The thickness and design lift coefficient of each section is put into the subroutine and the effective angle of attack is calculated using the guessed induced velocity. This allows for the determination of the lift coefficient. The drag data diagrams are not tabulated with respect to the angle of attack but rather the lift coefficient, meaning that the drag coefficient is calculated after the lift coefficient has been determined. The procedure of determining c_l and c_d is shown in Figure 3.13

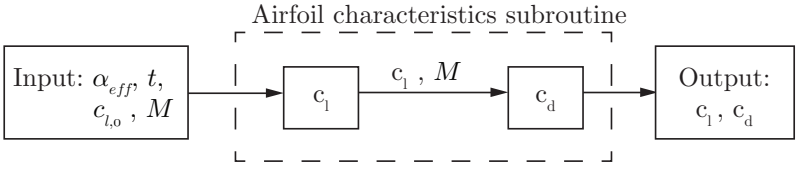

Figure 3.13: Procedure of calculating c_l and c_d from the digitized diagrams

The range of angles of attack may not be adequate for a wider off-design analysis. Therefore, the data range is extrapolated to include angles of attack from $-4°$ to $10°$, assuming the cases where the local angle of attack becomes lower than $-4°$ are of no interest in this thesis. For angles of attack larger than $10°$, correlations from the diagrams [21] are

used to determine the lift coefficients. From the correlations the lift coefficients increases linearly between 10° and 18° and above that assumes a constant value.

When determining the drag coefficients, the lift coefficients tabulated are ranging from 0 to 0.8. To include a larger range, the data is extrapolated down to -0.2 and correlations are applied when c_l exceeds 0.8.

3.2.3 Correcting lift and drag coefficients

As stated in Section 3.2.2 the data digitized was for airfoils with a design lift coefficient of 0.2. Data is available for a larger range but digitizing the data is a tedious process. Instead, a correlation factor for the airfoil characteristics was developed to account for varying design lift coefficient. The first approach for correcting the lift coefficient are adapted using Equations found in [27]

$$c_{l,corrected} = c_l + k_1^2 \left(c_{l,0} - 0.2\right) \tag{3.16}$$

This displaces the lift coefficient curves with respect to de input design lift coefficient. It was found that using $k_1 \approx 0.9$ yielded satisfactory results for $c_{l,0}$ ranging from 0 to 0.5 which was taken to be an adequate range. The correlation factor was determined by examining diagrams from NACA profiles with constant thickness but varying design lift coefficient. The correlation from Equation 3.16 is good in the subsonic range but deviates more and more when approaching the transonic range. The higher order effects associated with the performance of airfoils in the transonic range is hereby not captured correctly and will call for a more elaborate correlation, or simply just digitizing all the lift coefficient data. For this thesis, the maximum tip speed of the blades at take-off conditions will reach around Mach 0.6 for which the correlation is deemed satisfactory since the flow is not in the transonic range.

The drag coefficients are corrected in a similar manner. Firstly, a second correction is applied to the corrected lift coefficient used to find the drag coefficient. Thereafter, a correction is applied to the calculated drag coefficient to achieve a minimum drag position at a given angle of attack.

$$c_{l,calc} = c_{l,corrected} - k_2 \left(c_{l,0} - 0.2\right) \tag{3.17}$$

$$c_{d,corrected} = c_d(c_{l,calc}) + k_3 \left(c_{l,0}^2 - 0.2^2\right) \tag{3.18}$$

where Equation 3.17 corrects the drag with respect to the point of minimum drag, to make a symmetric drag correlation with respect to angle of attack. Equation 3.18 then applies a correction which increases the drag with respect to the design lift coefficient. A higher design lift coefficient means that the airfoil will generate more lift, hence more induced drag is formed since induced drag is dependent on lift [9]. The coefficients are found by correlating drag coefficient curves for constant airfoil thickness and varying

design lift coefficients and found to be $k_2 \approx 0.9$ and $k_3 \approx 0.0017$. Note that Equation 3.17 only serves as a correction variable and does not reflect the actual lift coefficient output.

Furthermore, the tabulated data from the report is taken from experiments performed at a certain flow velocity and hence a specific Reynolds number, which from the report is stated to be around 1×10^6 [21]. The Reynolds number at the model scale is significantly lower and therefore a Reynolds number correction should be applied. A simple method for correcting the airfoil characteristics using the Reynolds number is suggested by Yamauchi et al. [30]. For the drag coefficient, the correlation can be written

$$c_d = c_{d,t}/K \tag{3.19}$$

where $K = f(Re_t)/f(Re)$, the subscript t denoting tabulated data. The functions depending on the Reynolds number can be derived from flat plate theory and incorporate laminar or turbulent boundary layer theory. Skin friction, caused by shear stresses in the boundary layers along the airfoil surfaces is a large contributor to the overall drag in the subsonic range [8]. The effect is dependent on the characteristics of the flow and hence connected to the Reynolds number [9]. When the flow is completely laminar, the boundary layer starts growing along the surface of the airfoil and the shear stresses are relatively low since the velocity gradients are small [14]. As the flow gains speed over the surface of the airfoil, the velocity gradients increase and the flow makes a transition from laminar to turbulent. When the flow becomes turbulent, the shear stress at the wall will increase due to the increasing velocity gradient [14]. A couple of simple relations are adopted from the report by Yamauchi et al. [30].

$$f(Re) = Re^{-0.5} \tag{3.20}$$

$$f(Re) = Re^{-0.2} \tag{3.21}$$

$$f(Re) = Re^{n} \tag{3.22}$$

where Equation 3.20 is the laminar flat plate correlation and Equation 3.21 is a the corresponding correlation for turbulent conditions. Having no information about how the flow behaves in terms of transition from laminar to turbulent, an arbitrary correlation given by Equation 3.22 would be preferable. After trial attempts, an exponent of -0.6 was adopted. It produced trends that coincided well with experimental data from [28] at higher advance ratios, see Section 4.1. The Reynolds number correction has only been applied to the drag coefficient assuming that the effects of skin friction, which increases the drag are predominant with changes in Reynolds number compared to the effects on the lift coefficients.

3.2.4 Verifying method against experimental data

An aerodynamic design code was developed in Matlab® to calculate the performance characteristics of the chosen reference model propeller. The main purpose of this code

is to validate the airfoil characteristic subroutine which will be used in the aerodynamic analysis of the box-bladed propeller, described in Section 3.3

The reference propeller code was developed in steps to see the trends on performance as more flow features and effects were added to the code. Firstly, the method was written applying the Simple BET described in Section 2.3.1. Thereafter, induced axial velocities was introduced in concordance with the flow model described in Section 2.3.3. As the last step, corrections for design lift coefficients and Reynolds number was introduced[3].

3.3 Box-blade aerodynamic analysis method

The aerodynamic analysis method for the box-blade is developed in Matlab®, using a step-by-step methodology similar to the geometrical design method, see Section 3.1. The stacking line is defined with the desired geometric properties as for the geometry design, using Equations 3.2 through 3.4. Next, the ADP is defined by specifying any two of the following variables: desired flight speed V_∞, the rotational velocity or the advance ratio J. A subroutine then calculates the design point constants; the blade angle β, the convergence angle γ, the leading edge points and trailing edge points along the stacking line. The off-design analysis can now be initiated and is written in the same manner as for the reference propeller.

The main difference compared to the reference aerodynamic analysis is the definition of flow conditions. In the box-blade method, the equations are implemented using vectors rather than angles as for the reference propeller method. The flow field is described by vectors in 3D cartesian space and sectional lift- and drag coefficients calculated at each local profile plane are projected in the effective thrust and torque directions. In this manner, the vectors defined in the geometrical generation in Section 3.1.3 can be utilized in the aerodynamical analysis and the changes in flow angles can be accomplished solely by recalculating the relative velocity vector.

3.3.1 Method development

The box-blade aerodynamic analysis method structure is outlined in the flowchart depicted in Figure 3.14. It is basically written in the same manner as for the reference propeller with the difference that the flow field and geometry is defined in three-dimensional cartesian space rather than two-dimensional as for the case of the reference propeller.

The airfoil characteristics are computed using the same subroutine as for the reference propeller, with the effective angle of attack calculated at off-design points using Equation 3.11. The direction of the lift and drag forces are defined by vectors already available from the geometrical layout in Section 3.1.3. From Figure 2.7 regarding the modified BET method described in Section 2.3.1, it is observed that the sectional drag vector is

[3]Characteristic length for the Reynolds number is the chord length

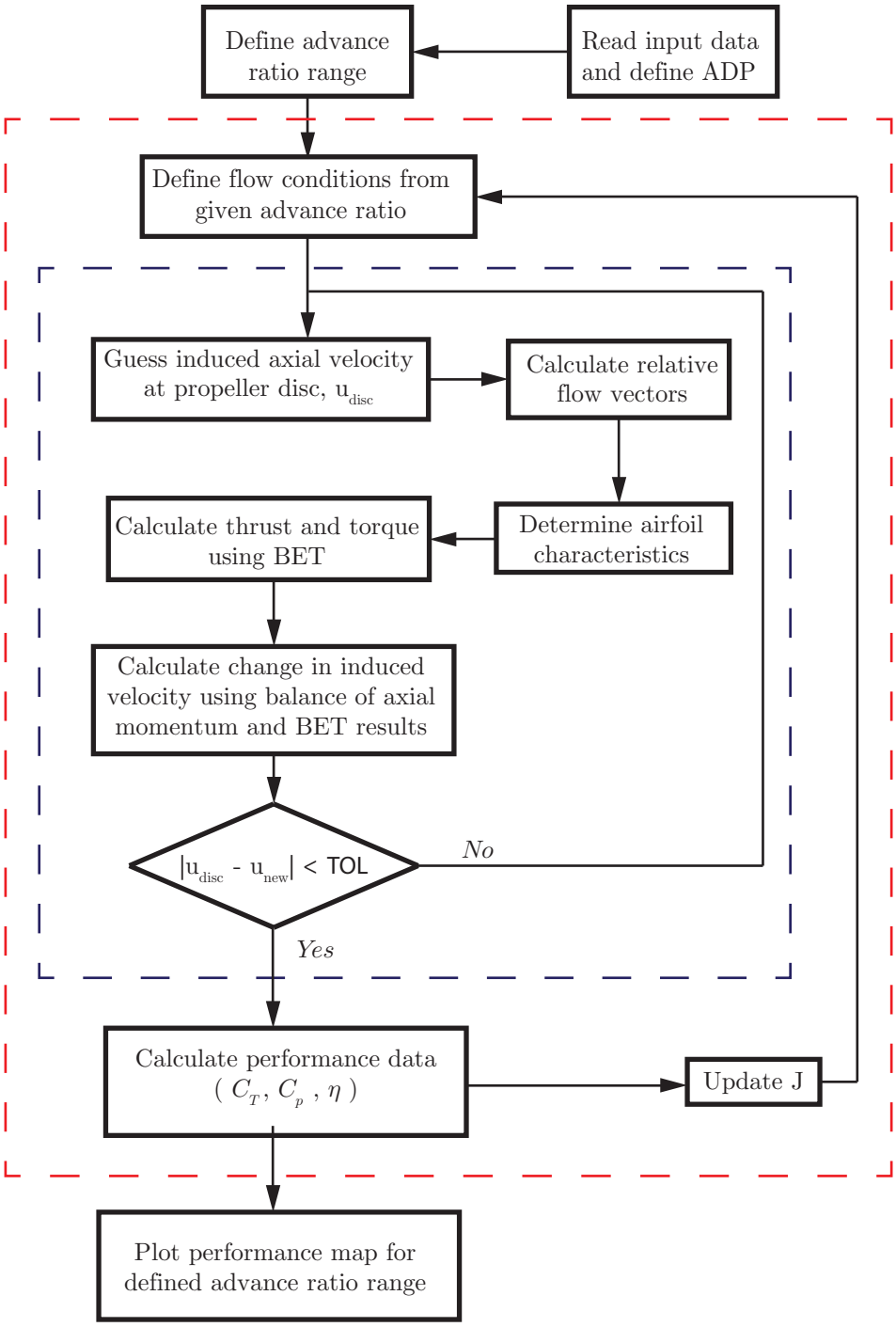

Figure 3.14: A flowchart outlining the calculation procedure of the box-blade aerodynamic analysis

parallel to the relative velocity vector and the lift vector is perpendicular to the drag vector. This implies that the cross product of the relative velocity vector and the local profile plane normal vector will form the sectional lift vector

$$\hat{\mathbf{e}}_{drag} = \hat{\mathbf{e}}_v$$
$$\hat{\mathbf{e}}_{lift} = \hat{\mathbf{e}}_v \times \hat{\mathbf{e}}_{pn}$$

By defining the thrust direction as the vector in the axial direction $\hat{\mathbf{e}}_{axial} = [\ 1\ 0\ 0\ ]$ and the torque direction as the vector made up by the two components ($y-$ and z-component) of the rotational velocity, the sectional lift- and drag coefficients can be projected in the thrust and torque-producing directions.

From this, the thrust and torque relations defined by Equations 2.14 and 2.15 can be rewritten

$$dT = q_R\,[\ c_l\ \hat{\mathbf{e}}_{lift,axial} + c_d\ \hat{\mathbf{e}}_{drag,axial}\ ]\ \ c\ dr \tag{3.23}$$
$$dQ = q_R\,[\ e_t \cdot (c_l\ \hat{\mathbf{e}}_{lift,rot} + c_d\ \hat{\mathbf{e}}_{drag,rot})\ ]\ \ c\ r\ dr \tag{3.24}$$

Note that the sectional torque is calculated by summing the rotational contribution and computing the scalar product of that addition and the tangential vector in each stacking line point, since the rotational vector is directed in an arbitrary direction in the rotational plane. When integrating, the radius can no longer be used for the integration boundaries. Instead, a stacking line arc length parameter dl is constructed and the forces are integrated along the length of the arc. Rewriting Equations 2.16 and 2.17 with the new integration limits give

$$T = B\int_{s=-1}^{s=1} dT\ \frac{dl}{ds}ds = B\int_0^{l_{stack}} dT\ dl \tag{3.25}$$

$$Q = B\int_{s=-1}^{s=1} dQ\ r\ \frac{dl}{ds}ds = B\int_0^{l_{stack}} dQ\ r\ dl \tag{3.26}$$

where l_{stack} is the length of the stacking line from the first blade root to the second blade root. The arc length parameter is constructed by starting at the first stacking line point, situated at the first blade root and measuring the distance to the next point. The distance dl is added to a vector named "StackLength" at the corresponding position. The procedure is repeated for each stacking line point and will create a vector which has the same number of elements as the specified number of blade elements. Numerical integration is then performed using the built-in Matlab® function `trapz.m` which utilizes the trapezoidal integration method.

3.3.2 Convergence study

From the methodology used to create the stacking line arc parameter dl, it is obvious that the arc lengths calculated between points are an approximation if a linear method is used. The larger the curvature is, the more the linear value will deviate from the actual arc length. A solution to this is increasing the number of elements along the stacking line, decreasing the local curvature of each element. This can however increase the computational time of the method greatly. To obtain an adequate number of elements for further studies, a convergence study was performed.

The aerodynamics code was run at static flow conditions for a varying number of stacking line elements. While the box-blade is designed at an ADP where the advance ratio is 1, the static condition will be very distant in off-design analysis and hence give a bigger deviation in results when varying the number of elements. The relative difference at a given element size is computed by taking the difference between the current solution of a performance variable and the old solution from the step before, divided by the old solution. The variable used for comparison is the coefficient of thrust C_T

$$\text{Relative difference} = \frac{C_T(N) - C_T(N-1)}{C_T(N-1)}$$

where n marks the current iteration with N elements and n-1 the previous iteration with N - ΔN elements. Running the code starting at 10 elements and increasing to 390 elements in increments of ΔN= 20 elements, the relative difference graph in Figure 3.15 is produced.

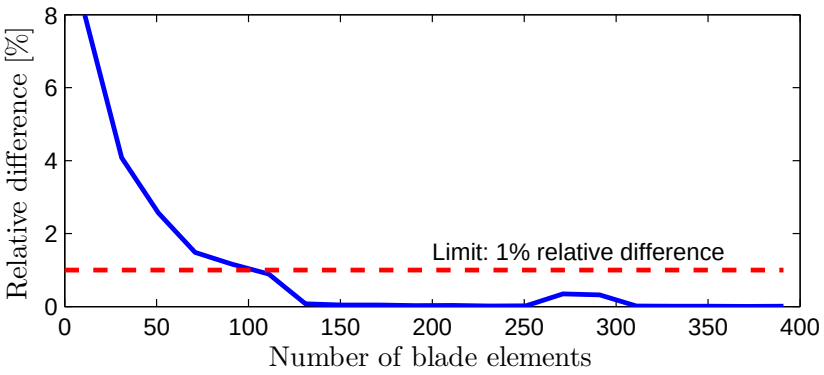

Figure 3.15: A convergence study comparing the difference in calculated coefficient of thrust with respect to the number of blade elements

Observing the graph, the conclusion is that convergence regarding the set limit is reached when using $\approx$ 130 elements. The bump in the results between 250 and 300 elements is thought to be associated with the integration method, since the subfunction `trapz.m` is designed for a domain with a uniform discretization. Because of the way the stacking line is constructed, the blade elements will not be uniform since the curvature is not constant.

This will created a discrepancy when using fewer elements but observing Figure 3.15, the convergence is deemed satisfactory with the set limit. For the actual studies of the box-blades using the aerodynamic method, a number of 200 elements have been used throughout the work.

3.3.3 Applying parameters from the reference open rotor propellers

In order to improve the initial design, data from a couple of reference open rotor propellers developed in the 70's and 80's are applied to the box-bladed propeller concept. This is performed with modifications due to the fusing of the blade tips and geometrical definitions of the box-blade.

Observing the blade angles from the initial geometry and comparing with the axial displacement angle ϵ, it follows that the chord displacement angle ζ is close to zero at the blade roots. This part of the blade is not effective in terms of producing thrust. Rather, the focus should be directed to the blade area around 75% of the blade tip, which is commonly used to approximate the performance of propellers [10]. Here, the chord displacement angle should be set around zero. Moreover, the blade sectional parameters are quite different from the manufactured propeller.

Adapting GE36 chord distribution to the box-blade

The chord distribution from the GE36 is translated into dimensionless form dependent on the diameter and fitted to the box-bladed model size. A way to scale the chord correctly with the diameter is to use the Activity Factor, a kind of effective area for a propeller blade. The activity factor, abbreviated AF, is defined by the following equation [31]

$$AF = \frac{10^5}{D^5} \int_{R_{hub}}^{R_{tip}} c \left(\frac{r}{R_{tip}}\right)^3 dr \tag{3.27}$$

For the box-bladed propeller with the GE36 chord distribution yields an AF of 275.8 for onee box-blade which amounts to ≈ 137.9 if the two blade-halves are "parted". The activity factor for one GE36 front rotor blade (conventional propeller) is 147. Since the GE36 rotor has 8 blades and the box-prop is designed with 5 box-blades, i.e. 10 single blades, the AF is rescaled like so

$$AF_{single} = \frac{8 \times AF_{GE36}}{10} = \frac{8 \times 147}{10} \approx 117.6 \tag{3.28}$$

which is the target AF for a single blade in the box-bladed configuration to match the GE36 total AF. Through iteration, by decreasing the chord using a constant, the correct AF can be reached.

3.4 Box-blade mechanical analysis method

Herein, the method for mechanical assessment is described. It should be noted that the mechanical assessment has been performed using the elementary theory described in Section 2.5 which is rather coarse for this rather complex structural problem.

3.4.1 Defining mechanical reference geometry

The geometry used in the mechanical module of the design method is constructed in the same way as the geometrical and aerodynamic methods, see Section 3.1.3. The main difference lies in the definition of coordinate systems and reference points. For the geometry, all related vectors are built with the stacking line as reference point. When it comes to the mechanical assessment, the center of gravity is the point of interest. Hence, the center of gravity for each local profile must be computed to contruct a center of gravity line, $\mathbf{X}_{cg}$. For the NACA 16-airfoil, a couple of easy correlations can be used to find the center of gravity [32]

$$x_{cg} = 0.482\ c \tag{3.29}$$

$$y_{cg} = 0.046\ c\ c_{l,d} \tag{3.30}$$

Furthermore, in order to facilitate calculations of the stresses and moments, the profile area $A_{profile}$ and the second moment of area I is computed in the subroutine used for profile coordinate generation. Equations 3.31, 3.32, and 3.33 are adapted from [33] and assumes that the bending of the airfoil will occur in the z-direction, which is equivalent to out-of-plane bending

$$A_{profile} = \int_0^c \left[Z_{upper} - Z_{lower}\right] dx \tag{3.31}$$

$$\overline{z} = \frac{1}{A} \int_0^c \frac{1}{2} \left[Z_{upper}^2 - Z_{lower}^2\right] dx \tag{3.32}$$

$$I = \int_0^c \frac{1}{3} \left[Z_{upper} - \overline{z})^3 - (Z_{lower} - \overline{z})^3\right] dx \tag{3.33}$$

Equation 3.32 computes the neutral surface of the airfoil section used when computing the bending of the profile, which will pierce the center of gravity if the line is assumed parallel with the chord line. Figure 3.16 shows an arbitrary section with center of gravity and the neutral surface defined.

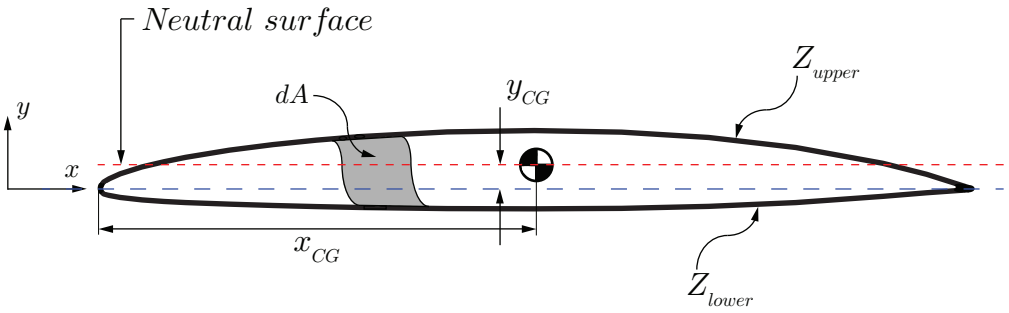

Figure 3.16: Center of gravity point, neutral surface and area of a NACA 16-airfoil

With the center of gravity line $\mathbf{X}_{cg}(s)$ defined, the tangential vectors along the line can be computed in the same manner as Equation 3.5, giving the unit tangent vectors for the center of gravity line.

$$\hat{\mathbf{e}}_{t,cg} = \frac{d\mathbf{X}_{cg}}{ds} \Big/ \left| \frac{d\mathbf{X}_{cg}}{ds} \right| \tag{3.34}$$

The purpose of the tangent vectors for the center of gravity line is, in the same manner as for the stacking line, to define local coordinate systems. The local coordinate system defined in this case has to to with the bending of beams and will be defined by three components; in-plane, out-of-plane and torsional direction. The torsional direction is readily defined by the unit tangent vector $\hat{\mathbf{e}}_{t,cg}$. The in-plane and out-of-plane directions can be defined by the methodology used in Section 3.1.3. The in-plane directions are defined by the directions of the local profile chords. However, when the blade is swept the chord can be smaller or larger than the aerodynamic chord laid out in Section 3.1.3, as illustrated in Figure 3.17

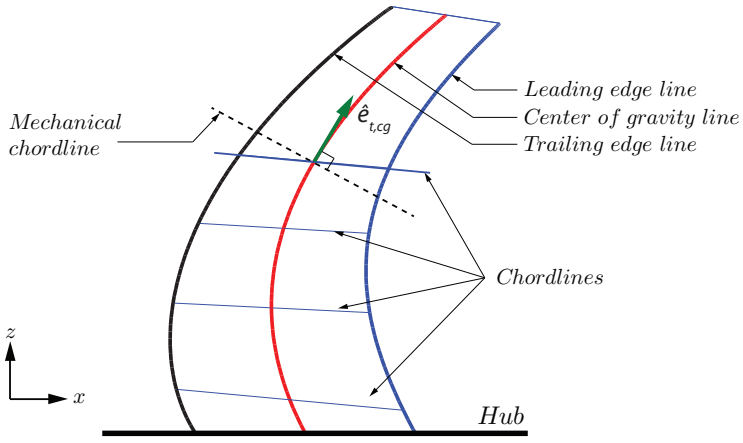

Figure 3.17: Planar view of a box-blade with chords from geometry and the definition of the mechanical chord using the tangent vector

The in-plane vector, or "mechanical chord" is constructed in the same manner as the local profile normal vector in Section 3.1.3 using the chord vector and tangent vector to the center of gravity line.

$$\hat{\mathbf{e}}_{in-plane} = \frac{\hat{\mathbf{e}}_{chord} - \hat{\mathbf{e}}_{t,cg}\left(\hat{\mathbf{e}}_{chord} \cdot \hat{\mathbf{e}}_{t,cg}\right)}{|\hat{\mathbf{e}}_{chord} - \hat{\mathbf{e}}_{t,cg}\left(\hat{\mathbf{e}}_{chord} \cdot \hat{\mathbf{e}}_{t,cg}\right)|} \tag{3.35}$$

The out-of-plane vector is then simply defined by the cross product of the torsional vector and in-plane vector. This forms the local direction vectors for the airfoil at each point, for which beam theory might be applied. The vectors are depicted in Figure 3.18.

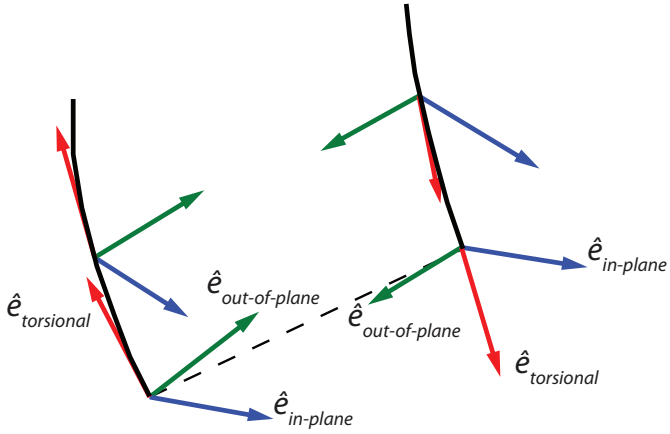

Figure 3.18: In-plane, out-of-plane and torsional directions - local beam coordinates for the box-blades

3.4.2 Applying forces

As mentioned in Section 2.5.1, the forces applied on the box-blade are the inertial forces. The total inertial force of a box-blade may be calculated in the following way

$$F_{inertia} = \int_0^{l_{cg}} \omega^2 \, r_{cg} \, dm = \int_0^{l_{cg}} \omega^2 \, r_{cg} \, \rho_{blade} \, A_{mech} \, dl_{cg} \tag{3.36}$$

where ρ_{blade} is the density of the material of the propeller blades and A_{mech} is the mechanical area which is the same as the in-plane area, computed by projecting the profile area onto the plane made up by the local mechanical coordinates defined in Figure 3.18. Each contribution to the force can be seen like putting a point mass dm at the local profile coordinate, compute the inertial force from that point mass and add the contributions together. The force directions are in the rotational plane, the yz-plane by the global convention used in this work. Figure 3.19 shows the contributions to the total inertial forces for 10 points along the center of gravity line for a symmetric, axially aligned profile.

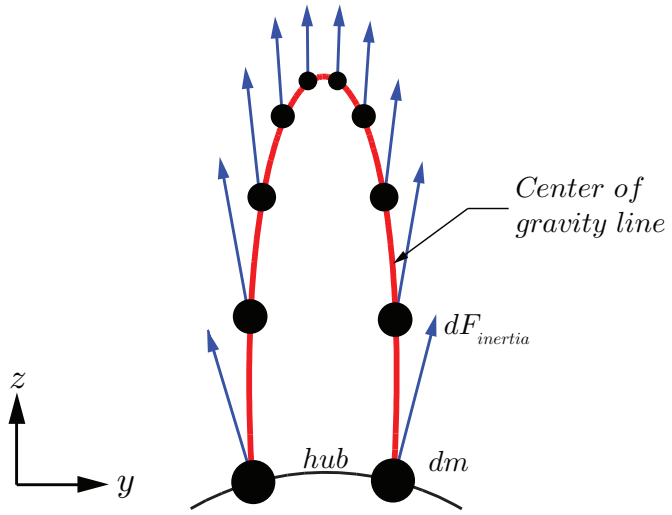

Figure 3.19: Force contributions for 10 points along the cg-line

No moments are applied to the blade. Calculating the total inertial force for a test propeller made in the ULTEM 9085 material, which has a density $\rho_{blade} = 1340\ [kg/m^3]$, the total force on one box-blade amounts to 1527.4 N at the ADP (26 000 RPM).

3.4.3 Computing shear forces

From classic beam theory it is readily deduced that the problem is indeterminate. With both blade ends fixed to the hub, one must make an approximation regarding the moments and reaction forces.

As suggested in Section 2.5.2, the desire is to minimize the root bending moment. As a starting point, no moment is applied at the fixed ends; the blade roots. Furthermore, the reaction force is assumed to be half the total inertial force which in the case of the ULTEM 9085 propeller amounts to 763.7 N meaning that the box-blade roots share the total load equally. By cutting the blade across the CG-line, the sectional shear forces and moments in each section of the blade can be computed.

3.4.4 Computing stresses and safety factor

The stresses in the blade can be computed using the shear forces calculated in Section 3.4.3 and the mechanical area A_{mech} defined in Section 3.4.2

$$\sigma = \frac{\mathbf{F}_{inertia}}{A_{mech}} \tag{3.37}$$

which may be projected in the normal direction, considering a section of the blade, and along the surface of that section, the transverse direction using the local coordinate vectors defined in Section 3.4.1, where the normal direction is defined by $\hat{\mathbf{e}}_{normal} = \hat{\mathbf{e}}_{torsion}$ and the transverse direction is defined as $\hat{\mathbf{e}}_{transverse} = \hat{\mathbf{e}}_{in-plane}\hat{\mathbf{e}}_{out-of-plane}$

$$\sigma_{normal} = \sigma \cdot \hat{\mathbf{e}}_{normal} \tag{3.38}$$

$$\sigma_{transverse} = \sigma \cdot \hat{\mathbf{e}}_{transverse} \tag{3.39}$$

Furthermore, the effective von Mises stress is computed.

$$\sigma_{vM} = \sqrt{\frac{1}{2}\left[(\sigma_1 - \sigma_2)^2 + (\sigma_1 - \sigma_3)^2 + (\sigma_2 - \sigma_3)^2\right]} \tag{3.40}$$

where σ_1, σ_2 and σ_3 are the stresses in the principle direction, i.e. the local beam coordinate directions defined in Section 3.4.1. Comparing with the tensile strength of the material, a safety factor against rupture can be approximated by comparing with the maximum effective stress

$$\text{SF} = \frac{max(\sigma_{vM})}{\sigma_{UTS}} \tag{3.41}$$

where σ_{UTS} signifies the ultimate tensile strength of the material. This is only valid when considering an even stress distribution and no stress concentrations. In reality, because of bending the actual safety factor is 2-3 times lower for a well designed blade with small bending moments.

3.4.5 Computing bending moments

As described in Section 2.5.3, the theory behind curved beams with arbitrary geometry is rather complicated and has no been investigated to further extent in this thesis.

3.5 Matlab design code

The three modules described in Section 3.1, 3.3 and 3.4 was developed as individual modules during the work. At the end of the thesis work, the modules were sorted and divided into subroutines. A main program was then written which calls the subroutines depending on the case investigated. A total of 15 subroutines are used for the three modules. For the geometry section, the subroutines will take simple input data about the desired propeller geometry, blade sectional data and aerodynamic design point.The program has the ability to output profile data which then can be imported into a CAD software.

The aerodynamic analysis module can be executed both for a static case, meaning a stationary propeller and a dynamic case simulating wind tunnel testing. The mechanical module specifies the desired material of the blades and computes the shear forces, principal stresses and lastly the effective stresses according to the von Mises criterion. A safety factor against rupture is also computed. A simple bending moment assessment has been implemented, but it should be taken lightly.

All data and plots can be saved as outputs in the program, and is governed by user inputs. The source code of the main program can be seen in Appendix C.

4

Result

In this chapter, the results obtained by using the geometric, aerodynamic and mechanical design methods developed during the thesis are presented. Firstly, the results from the reference propeller used to trim the airfoil characteristics subroutine are presented. Following is the results from a first prototype geometry used to verify the accuracy of the manufacturing method.

4.1 Aerodynamics of reference propeller

Here follows the results from the aerodynamic design method developed for the reference propeller in order to trim the airfoil characteristics subroutine. The results are presented in Figures 4.1, 4.2 and 4.3.

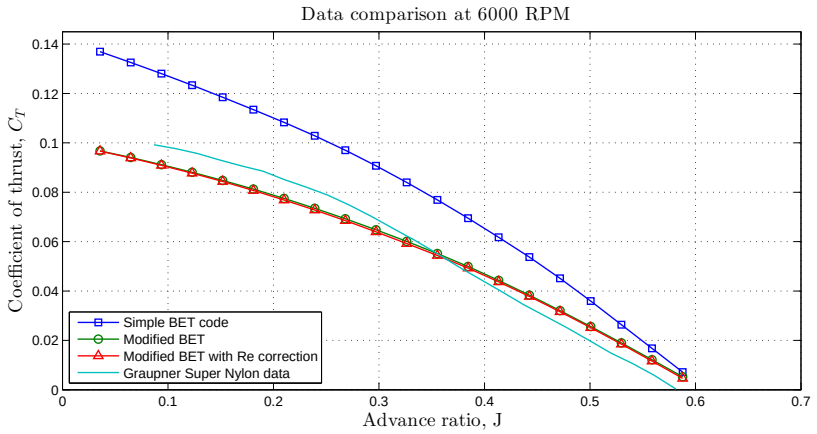

Figure 4.1: Coefficient of thrust for the method in various development stages compared with experimental data from [28]

From 4.1 it is seen that the modified BET with Reynolds number correction (triangle curve) has a relatively good concordance with the Graupner data (solid curve), with the best matching around an advance ratio of 0.35. Furthermore, it is interesting to see that the Reynolds number correction has little effect on the thrust, since curves showing the modified BET both with and without Re-correction are almost identical.

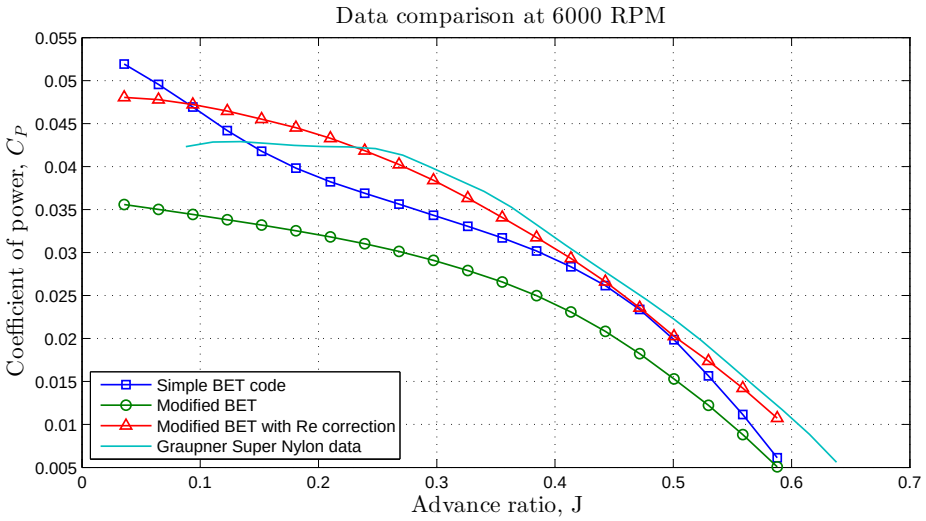

Figure 4.2: Coefficient of power for the method in various development stages compared with experimental data from [28]

Observing the coefficient of power in Figure 4.2, the simple BET method actually performs close to the Graupner data but with a different trend. The introduction of induced velocities lowers C_P greatly but the correlation improves when applying the Reynolds number correction. To be noted is that the exponent for the correction factor used in Equation 3.22 is chosen to get a good matching of the curves at higher advance ratios rather than at static conditions.

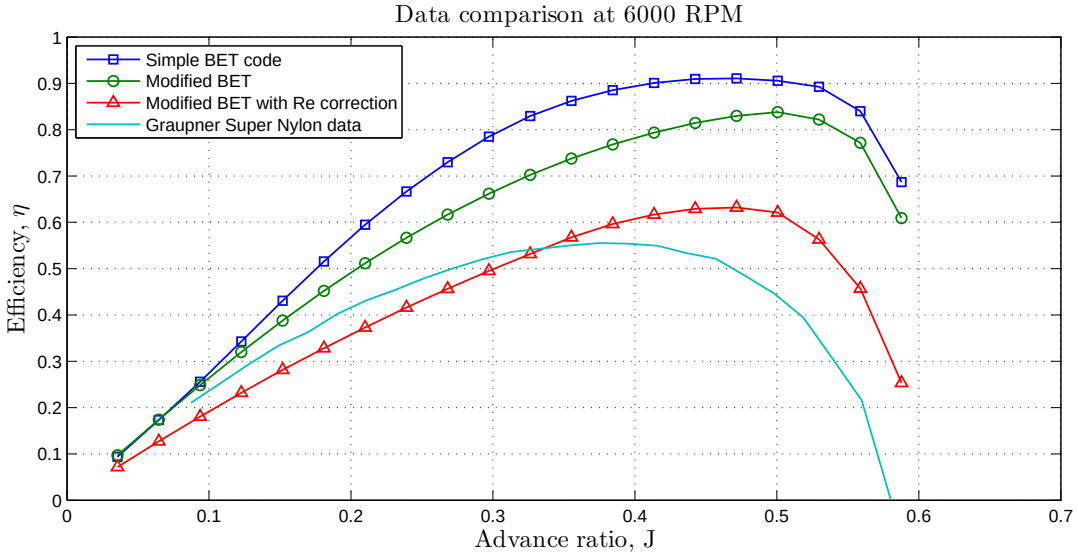

Figure 4.3: Efficiency for the method in various development stages compared with experimental data from [28]

Lastly, the efficiency is highly overestimated for the simple BET method in 4.3. It approaches the Graupner data with added induced velocities and is further decreased when introducing Reynolds number correction. To be noted is that the efficiency coincides with the test data at an advance ratio close to 0.34 which is analogous with the coincidence for the thrust data.

4.2 First box-bladed propeller results

Herein, the geometry of the first box-bladed prototype designed and manufactured in this thesis is presented. Following are the results from the aerodynamic and mechanical evaluations of said geometry.

4.2.1 The first and manufactured box-blade geometry

The first box-bladed propeller was designed mainly to test out the manufacturing method and not with testing in mind. Hence, the blade is not aerodynamically and mechanically optimized. Rather, the geometric and blade section parameters have been given plausible values. The parameters for the first box-bladed propeller prototype are presented in Tables 4.1, 4.2 and 4.3. For the blade section data, the distributions are shown more explicitly in Figure 4.4

Table 4.1: Geometric data for the first box-bladed prototype

Stacking line geometry	
Diameter [m]	0.15
R_{hub}/R_{tip}	0.4
Number of box blades, B	5
Axial displacement angle, ϵ	45
Chord displacement angle, ζ	0
Blade root distance, l_{root}	$0.2 \times R_{tip}$
Forward sweep distance, l_{sweep}	$0.2 \times R_{tip}$

Table 4.2: Aerodynamic design point data for the first box-bladed prototype

Aerodynamic Design point data	
Rotational speed [RPM]	26,000
Induced Advance ratio J_{ind}	1
Resulting flight speed [m/s]	65

Table 4.3: Blade section data for the first box-bladed prototype

Blade parameters			
	Leading root	Tip	Trailing root
Chord, c/D [%]	18.6	9.3	18.6
Thickness, t/c [%]	12	8	12
Design lift coefficient, $c_{l,d}$	0.8	0	-0.8

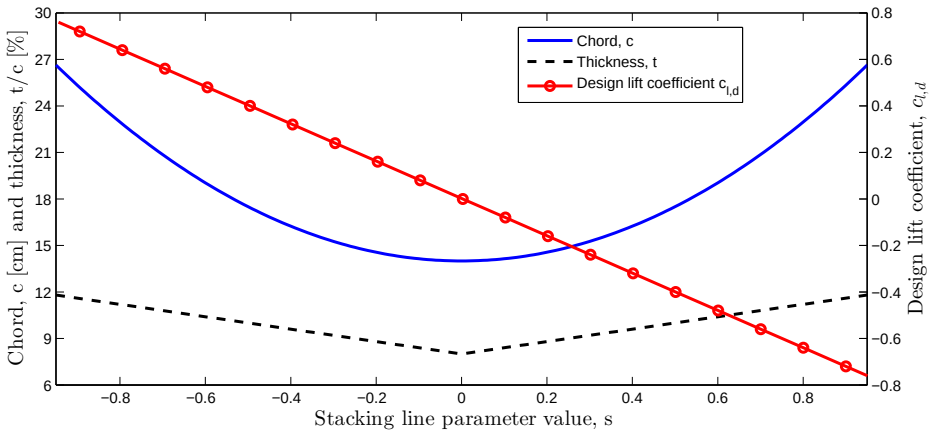

Figure 4.4: Chord-, thickness and design lift coefficient distribution for the manufactured box-blade

The data from Tables 4.1 and 4.2 are plugged into the geometry module in order to compute the blade angle, convergence angle, leading- and trailing edge chords. As mentioned in Section 3.1.3, the blade is in the a fixed pitch configuration, meaning that these variables are fixed. The distributions of blade- and convergence angle are shown in Figure 4.5

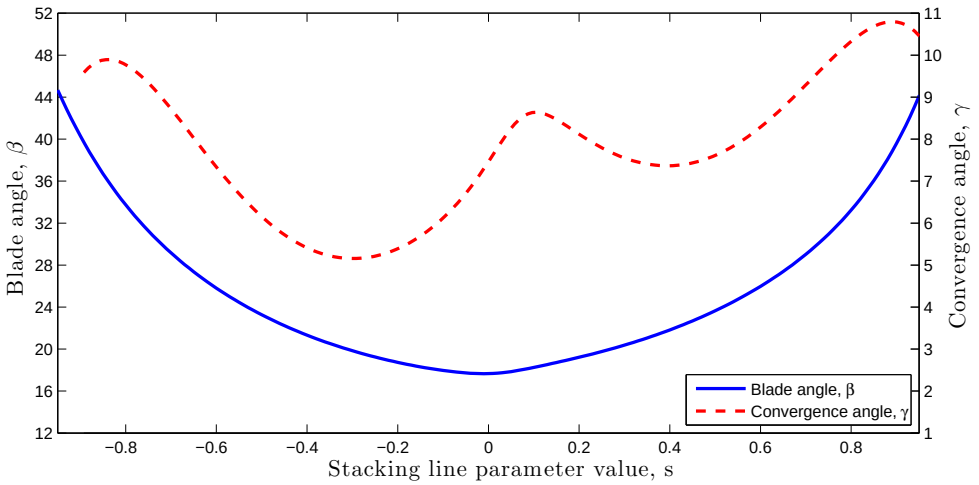

Figure 4.5: Blade angle and convergence angle the at specified ADP

With the blade angles, leading- and trailing edge points found, the profiles can be computed for each section and scaled/oriented according to the method described in Section 3.1.3. The input data from Table 4.3 is used and an initial angle of attack is added to the blade angle. The angle varies linearly from 5° at the blade roots to 0° at the blade

tip, where the stacking line parameter reaches 0. The resulting geometry is depicted in Figure 4.6

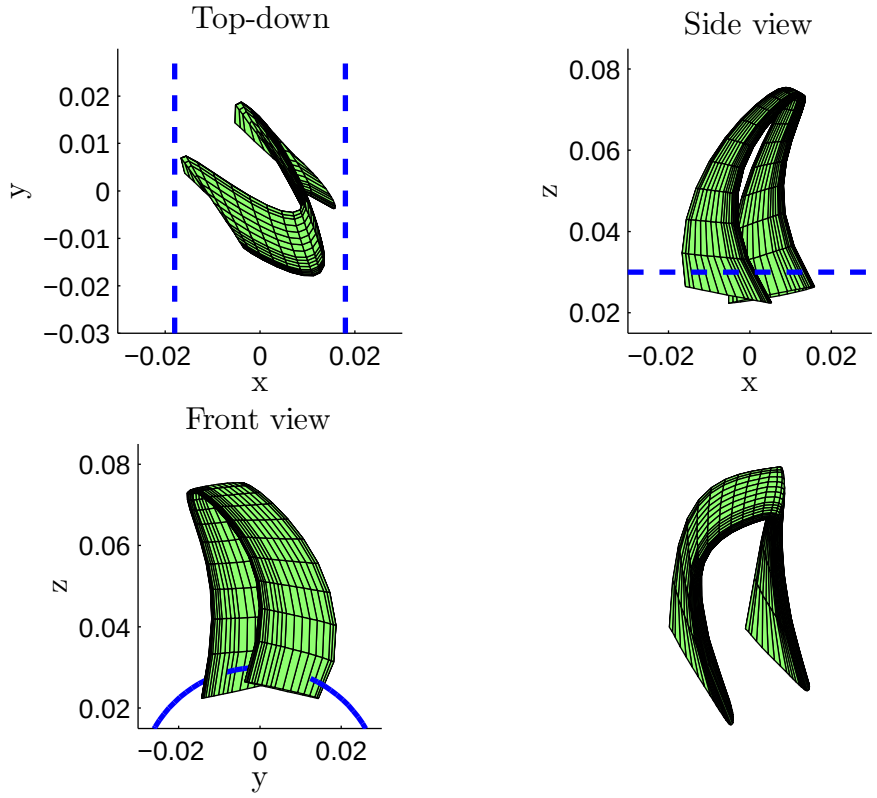

Figure 4.6: Final geometry output from Matlab that has been exported to a CAD software

The dashed lines in the 2D section views represent the hub. It can be noted that the blade actually extends into the hub. This is done due to the fact that the method described in Section 3.1.3 will lay out the chord lines with respect to the relative induced flow $V_{R,ind}$ at each point. Since the blade does not extend along a fixed radial line, the vectors will be directed in three dimensions according to the relative flow. If the stacking line begins at the actual hub radius, the leading edge might end up outside the hub radius and conversely with the trailing edge. This has to do with the choice to lay out the chord lines straight between the leading and trailing edge points.

Therefore, the blade geometry is constructed using a fictive hub radius which is smaller than the real hub radius, to ensure that the leading and trailing edge points of the root sections end up below the hub line. This may otherwise create problems when transferring the geometry to the CAD software Autodesk Inventor®. For the aerodynamic and mechanical assessment, the real hub radius is used. All data is then calculated with respect to the real hub and integration are made from points along the stacking line

which are situated closest to the hub.

A simple output script transfers the profile coordinates to the CAD software, where the profiles are modeled into a solid blade. A pre-made hub is then fitted to the blade geometry and the single blade is patterned rotationally to the five propeller blades of the actual propeller. A close up of one of the solid blades fitted to the hub is seen in Figure 4.7a and the entire propeller model is shown in Figure 4.7b

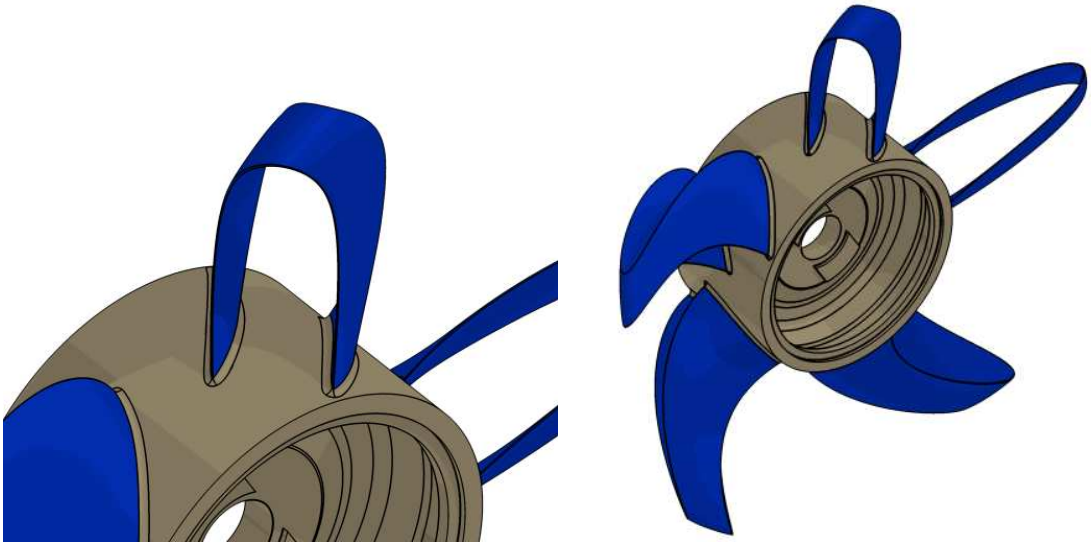

(a) Close-up of a blade **(b)** The finished propeller prototype

Figure 4.7: Manufactured propeller prototype in the VeroGrey material mounted in the rig

The hub is designed by the other thesis worker involved in the project [2] in order to allow attachment to the motor shaft of the test rig. The hub has a diameter of 60 mm and a width of 34 mm at the interface surface between the blade and hub. For the manufacturing, fillets are added between the hub and box-blades which can be observed in Figure 4.7a.

The finished prototype is manufactured in two different polymeric materials, using two Rapid Prototyping techniques; one prototype is made in the ULTEM 9085® material using an FDM[1] method and the other is made in the material VeroGrey® using a PolyJet method [34]. The prototypes are manufactured by Digital Mechanics AB in Vasterås, Sweden. The main difference between the manufacturing methods are the layer thicknesses attained. For the FDM material, the layer thickness is 0.254 mm and the PolyJet method achieves a layer thickness of 0.016 mm. This may prove to have

[1]Fused Deposition Molding

effect on the aerodynamics, since surface roughness has a great influence on overall drag [14].

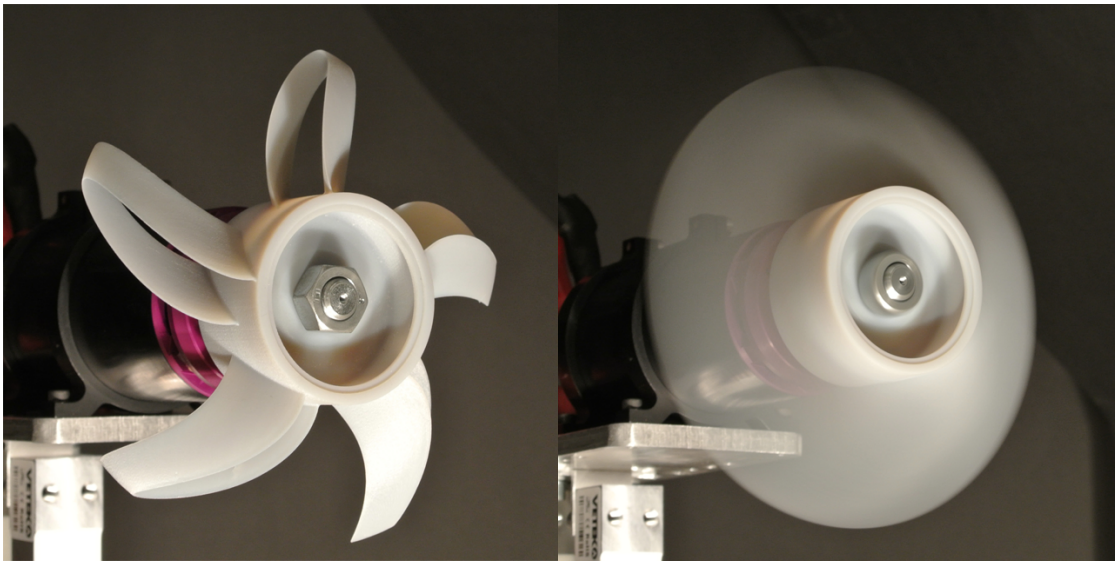

(a) Stationary **(b)** During tests

Figure 4.8: Manufactured propeller prototype in the VeroGrey material mounted in the rig

4.2.2 Aerodynamic performance of the first prototype

One of the objectives of the first prototype was to assess the tolerances and precision of the manufacturing methods. In addition, the geometry is run through the aerodynamic design module. Using the methodology described in Section 3.3, the performance parameters of the box-bladed propeller are computed; total thrust T, total resistance torque Q together with propeller efficiency. The calculations are made in two ways

- For static conditions, resembling the rig in a static environment
- For dynamic conditions, resembling tests made in a wind tunnel

To achieve the static conditions, the loop is performed assuming a flight speed $V_\infty = 0$ and varying the rotational speed from 1000 RPM to 26000 RPM in 25 increments. For the dynamic conditions one case with a constant rotational speed is assessed for different inflow conditions, ranging from 0 to 70 m/s using 25 increments. The results from the static runs are presented in Figure 4.9 and 4.10. The dynamic results are presented in Figures 4.11 and 4.12.

Static Results

From Figure 4.9, it can be seen that the coefficient of thrust increases at lower rotational speeds and then stabilizes. At higher rotational speed C_T increases more rapidly. For the coefficient of power, observing Figure 4.10 it is seen that C_P decreases for lower rotational speeds and is stabilized around a value of 0.94.

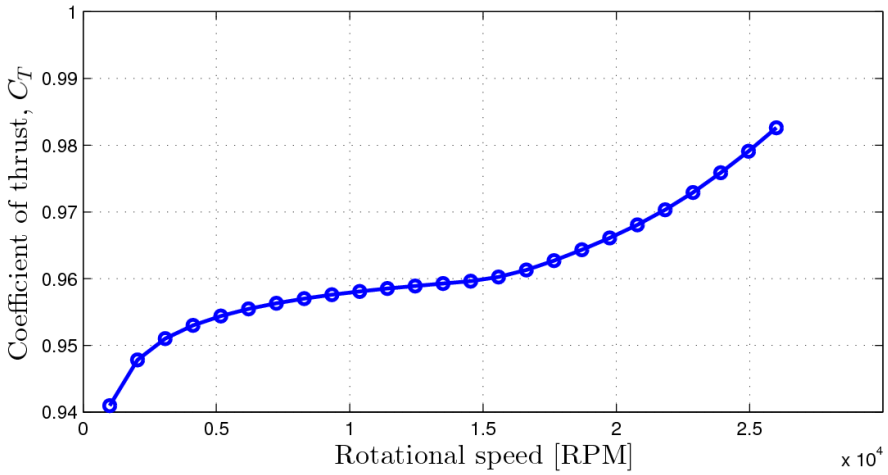

Figure 4.9: Coefficient of thrust for the static case

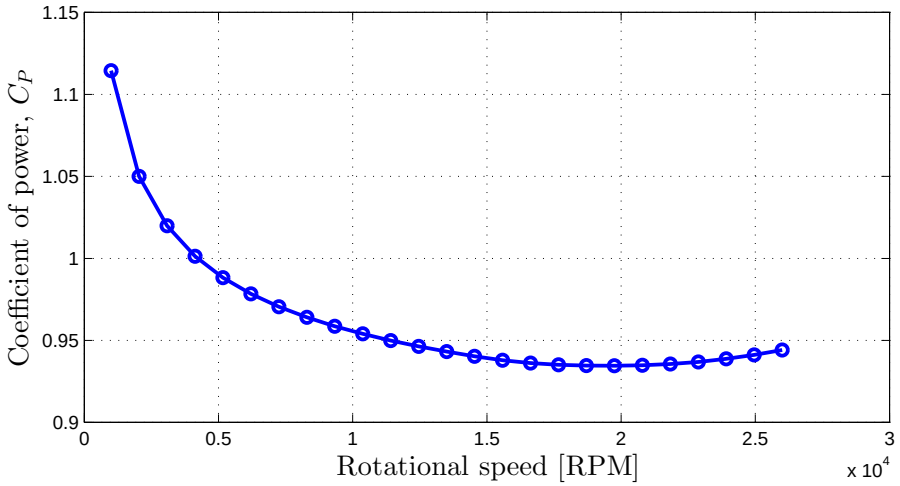

Figure 4.10: Coefficient of power for the static case

Dynamic Results

Coefficient of thrust

From Figure 4.11, on can observe that the coefficient of thrust is highest for static conditions, and declines as the advance ratio is increased. Comparing the conventional advance ratio J (marked by the curve with circles) and the calculated advance ratio due to induced velocities at the propeller disc, it can be observed that there is a significant amount of velocity passing through the propeller at static conditions yielding an induced advance ratio of ≈ 0.86.

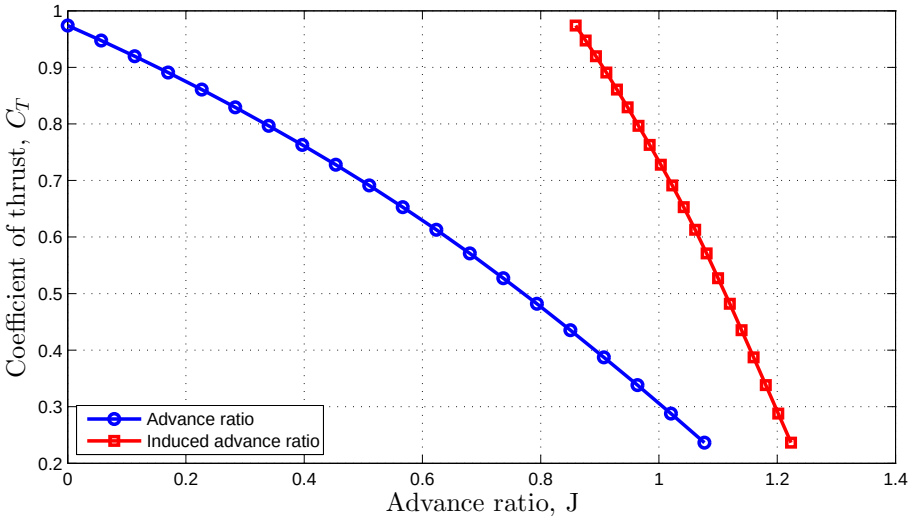

Figure 4.11: Coefficient of thrust for the dynamic case

Furthermore, with increasing flow velocities, the increase in the induced velocities has a smaller and smaller impact on the induced advance ratio compared to the advance ratio based on the true airspeed. The ratio between J and J_{ind} ranges from 1 for the static case, meaning that the induced velocities are 100% of the velocity moving through the propeller disc to $\approx 12\%$ for the case with a flight speed of 70 m/s.

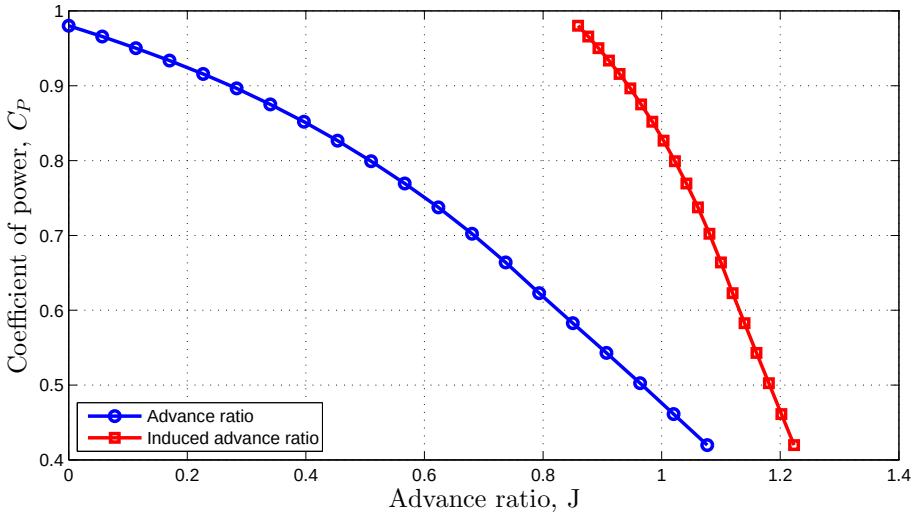

Figure 4.12: Coefficient of power for the dynamic case

Coefficient of power

From Figure 4.12 the trend is similar to that of the coefficient of thrust but with a somewhat steeper decline for higher advance ratios.

4.2.3 Mechanical assessment of the first prototype

Shear forces

From the structural analysis of the first box-blade, the shear forces along the blade computed according to Section 3.4.3 is depicted in Figure 4.13.

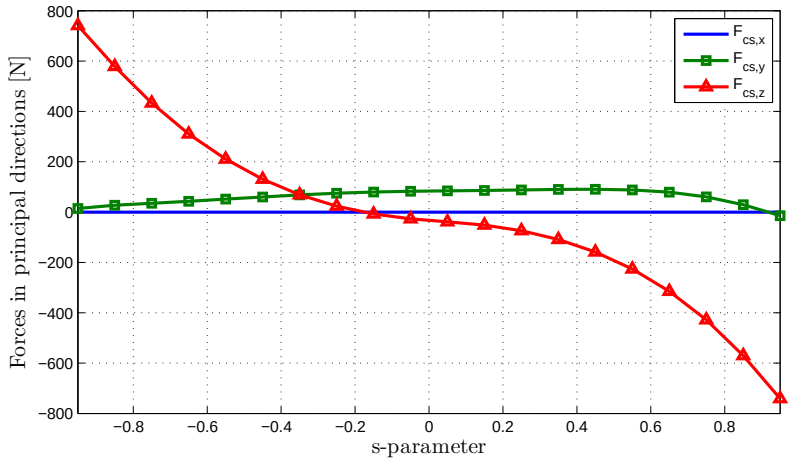

Figure 4.13: Shear forces along the blade in local blade coordinates

Observing Figure 4.13, it is seen that the shear stresses are zero in the x-direction . The stresses are largest in the z-direction, which is expected since the inertial forces, pulling the blade away from the hub, has the largest component in this direction. The forces in the y-direction are somewhat smaller, again related to the y-component of the inertial forces. The shear forces in the roots amounts to 763.7 N, which is concordant with the assumption that reaction forces are equal in the blade roots.

Principal stresses

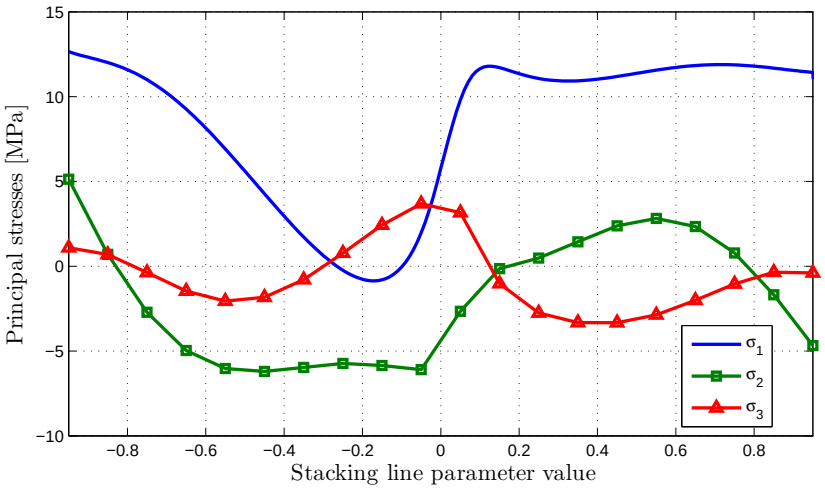

Figure 4.14: Principal stresses along the local blade coordinates

Figure 4.14 shows the principal stresses in the blade considering the shear forces. From theses stresses, the effective stresses according to the von Mises criterion described in Section 3.4.4 can be computed.

von Mises effective stress

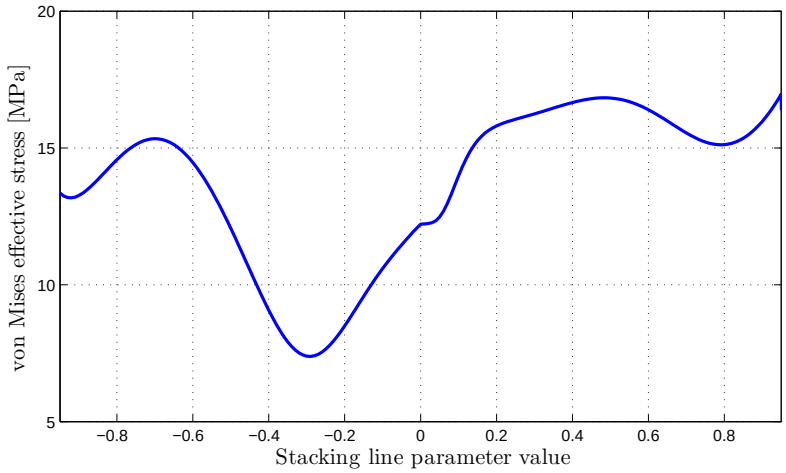

Figure 4.15: von Mises effective stress along the blade and safety factor against tensile rupture

The effective stresses are highest in a the middle area of the leading blade (with negative s-parameter) and at the trailing blade root. The maximum effective stress amounts to 19.73 MPa, which yields a safety factor against tensile rupture of ≈ 3.65.

Page left intentionally blank

5

Conclusion

This chapter will summarize the conclusions drawn from the thesis work. To be mentioned is that the main part of the work has consisted in method development which has resulted in a number of design codes which can be used for easy analysis of an arbitrary box-blade geometry. This makes the method one of the main focuses of the following discussions.

Firstly, the geometrical design method is discussed. After that follows the aerodynamic analysis method and thereafter, the structural assessment method is discussed. Finally, a couple of recommendations for future work are stated.

5.1 The geometrical design method

Design approach

The method which is used to design the preliminary geometry of the stacking line is in essence rather simple. This is a good approach when no immediate requirements on the geometry is specified, making the polynomial function approach a method with a lot of design freedom. However, the degree of control is somewhat restricted unless the individual using the design code knows exactly how to control the polynomial functions. The polynomial approach has been satisfactory for this particular work, since the design process has called for easy modifications of the stacking line at an early stage. To give more control to the stacking line layout the polynomials could be replace by or converted into functions with parameters that are governed by geometrical constraints, i.e. sweep angle and blade spacing.

Fixed pitch vs. adjustable pitch

The fixed pitch approach is a very principal design with little design freedom. Fixing the blade angles will cause the propeller to perform at its best around the given design point, which can be observed for the first box-bladed prototype in Section 4.2.3. Performance will be worse for off-design points in terms of efficiency. Rather, the approach would be to apply Equations 3.10 when computing the leading and trailing edge points, hence pitching the blade with respect to the relative flow field in each off-design flow case. This is analogous with having an adjustable pitch propeller, which is the case for practically every propeller today. Since the geometry in this work was mainly designed for use in simple model-scale testing, the adjustability of the propeller blades were not included because of the complexity of such a device.

Chord and profile layout

The layout of profile chords are greatly simplified. In this work, the chords are laid out in straight lines along the direction of the relative inflow, with and without angle of attack when applicable. This will create problems close to the hub, as mentioned in Section 3.1.3 and clearly visible in Figure 4.6. For the geometry, this has no immediate effect except for the fact that parameters for the roots have to be specified at the *actual* hub radius. This is facilitated in the code by using boundary nodes which essentially calculates the point on the stacking line closest to the hub at each blade end, saves the node numbers and uses these boundaries for all performance-governing purposes, i.e. integration of thrust, torque and stresses.

A more accurate method would be to lay out the chord lines along a cylindrical surface at the given stacking line point. This method will however increase the complexity of the profile stacking which then would need to be projected onto a cylindrical surface. It might very well prove to be a simple fix, but will create further problems when exporting to the CAD software. From experience, the profiles exported to Autodesk Inventor could not be defined in 3D space, even though the profiles were constructed on a given plane. The problem lies in that Inventor does not recognize arbitrary planes, so to convert the imported airfoil profiles to a solid geometry the working methodology consisted of

1. Import the first profile as a splined curve
2. Define a plane using three points on this curve
3. Project the splined curve onto the plane
4. Import the next profile

This can be very tedious work if the number of required profiles is large. As an example, the work to convert the 25 profiles exported for the first prototype into a solid blade consumed about 20 minutes of work. This might well be possible to do faster by writing

a script, but this was not investigated further since the procedure was only performed a couple of times during the thesis.

Coming back to the cylindrical stacking of the profiles, this will introduce larger errors in the actual geometry when using the methodology explained above, since the cylindrically laid out profiles will have to be projected onto a plane which is flat. A solution to these problems would be to investigate different ways to make the profiles into a solid model, perhaps by using a different CAD software.

5.2 The aerodynamical analysis method

As mentioned in Section 5.1, the chords are laid out straight between the leading and trailing edge points. This chord is also implemented in the aerodynamic analysis and does not reflect the actual aerodynamic chord. The approximation has however deemed sufficient for a first analysis, but when implementing methods that take higher order effects into account, e.g. the effective velocities due to the actual sweep angles of the blades, the chord layout becomes a greater concern. It has however been left to future work since this thesis does not take the effects of swept blades into account in the aerodynamic analysis.

Airfoil characteristics

The airfoil characteristics subroutine has been shown to yield satisfactory results but within a limited design range. The data gives good results when the flow produces angles of attack from -4° to $\approx 15^\circ$ degrees. This implies that, for a fixed pitch propeller designed at a high advance ratio, off-design analysis at lower advance ratios yields good results since the relative flow will produce positive angles of attack. For off-design at advance ratios higher than that defined by the ADP, the method is only implementing angles of attack down to -4°. If the angle of attack is below -4° it is kept constant. This will yield bad results when investigating flow cases that yield negative angles of attack. On the other hand, negative angles of attack means that the blades are producing negative thrust and hence brakes, which is only desirable in e.g. a landing situation, which is out of the scope of this thesis.

Correction of design lift coefficients

For the design lift coefficients, the results are satisfactory when the camber of the airfoils are ranging from 0 to 0.5. Above that, the correlations described in Section 3.2.3 causes larger deviations in performance. Furthermore, the correlations are bad when approaching the transonic region. For further studies, involving an ADP at e.g. cruise conditions, the data set need to be either corrected in a different way or more data has to be digitized. Another approach would be to implement the use of an optimization software, e.g. `XFOIL`. Said software can be connected to Matlab using an intermediate transfer script generating `XFOIL` input from the Matlab design method, calculate profile

characteristics and export the results back into the design method. This could however easily become a whole thesis in terms of amounts of work.

5.3 The structural assessment method

General methodology

The structural part of the thesis has been performed using very simplified theory for a rather complicated case. The choice to only implement the inertial forces on the blades was made because of time constraints. Also, a more complicated analysis of the forces and moments affecting the blade structure are more easily assessed using e.g. FEM methods. FEM was not considered in this work due to the fact that there is little or no data available for these kind of structures, and a first assessment using simple derivations of elementary beam theory proved a more suitable approach.

Shear forces and stresses

The forces and effective stresses produced from the inertial forces amounts to around 16 MPa (see Figure 4.15) for the first box-bladed prototype, again, only considering the stresses from shear forces and with the assumption that the reaction forces at the blade roots are equally distributed. Given this, the safety factors amounts to 4.24 which is rather high. This is however based on an ULTEM 9085 propeller with homogenous material properties under a simplified load case and should be given secondary thought.

5.4 Recommendations for future work

Geometry design method

For the geometry, the first and foremost recommendation for future work is investigating implementing the stacking line functions in such a way that better control of the blade angles, sweep angles, chord layout and convergence angles can be done. Moreover, the method could be extended to include the aft rotor of a co-axial open rotor configuration. The method would then need to be refined to give output data at the trailing edge of the front rotor, to provide input for the inflow of the aft rotor.

Aerodynamic analysis method

The introduction of the rotationally induced velocities is the first change that should be implemented into the aerodynamic design method. Contrary to the assumption made in Section 2.3.3, the rotationally induced velocities will generate a lot of swirl which translates into loss in performance. Adding this will further refine the aerodynamic analysis. Furthermore, the airfoil characteristics subroutine should be extended to include a larger data range. In addition, the subroutine should be rigorously verified, e.g. by investigating the performance of a number of model propellers from the UIUC database [28].

Verification of the aerodynamic analysis should also be made against the model scale testing performed with the box-bladed prototype when a sufficient set of data has been collected. This is to assure a statistically determinate result. CFD analysis should also be performed, to assess the higher order effects associated with the transonic operating range of the box-bladed propellers, e.g. tip vortices and blade interference effects.

Mechanical assessment method

For the structural part of the thesis, the first addition made should be an assessment of the bending moments of the blade at the ADP. Furthermore, a FEM analysis should be conducted to conclude if the results and those from the simple mechanical design method are in the same ballpark. Additionally, the introduction of forces omitted in this thesis, i.e. aerodynamic forces and vibrations should be implemented and assessed. Lastly, rigorous finite element analysis on a detailed level should be done in the near future, together with actual mechanical testing, verification and validation.

Bibliography

[1] A. Axelsson, A. Goransson, C. Hung, S. Klipic, J. Landahl, J. Olofsson, D. Thor, Developement of a box-bladed propeller - mechanical analysis and feasibility of the concept, Tech. rep., Department of Product & Production Development, Chalmers Univeristy of Technology (2012).

[2] F. Carlsvärd, Experimental rig design and testing of a box-bladed propeller, Master's thesis, Luleå Technical University, unpublished (2013).

[3] R. Avellan, A. Lundbladh, Air propeller arrangement and aircraft, Patent WO 2011/081577 A1 (December 2009).

[4] Fuel and Air Transport, A report for the European Commission, Air Transport Deparment, Cranfield Univeristy (2008).

[5] Clean Sky Research Project webpage - SAGE demonstrators, `http://www.cleansky.eu/content/page/sage-demonstrators`, accessed: 2013-02-06.

[6] D. Van Zante, Re-establishing open rotor as an option for significant fuel burn improvements, `http://www.aeronautics.nasa.gov/pdf/asm_presentations_open_rotor`, Research Presentation.

[7] L. Prandtl, Induced drag of multiplanes, National advisory committee for aeronautics technical note no. 182 (March 1924).

[8] I. Kroo, Nonplanar wing concepts for increased aircraft efficiency, Tech. rep., Stanford Univeristy CA (2005).

[9] J. D. Anderson, Fundamentals of Aerodynamics, 3rd Edition, McGraw-Hill Companies Inc., 2001.

[10] E. Torenbeek, H. Wittenberg, Flight Physics - Essentials of Aeronautical Disciplines and Technology, with Historical Notes, Springer Dordrecht Heidelberg.

[11] M. Cook, H. D. Curtis, F. De Florino, A. Filippone, L. Jenkinson, J. Marchman, T. Megson, M. Tooley, J. Watkinson, D. Wyatt, Aerospace Engineering Desk Reference, Elsevier, 2009.

[12] E. Torenbeek, Synthesis of Subsonic Airplane Design, Delft Univeristy press, Delft, the Netherlands, 1982.

[13] AMME University of Sydney, Aerodynamics for students: Analysis of propellers, `http://www-mdp.eng.cam.ac.uk/web/library/enginfo/aerothermal_dvd_only/aero/propeller/prop1.html`, accessed: 2012-10-15.

[14] F. M. White, Fluid Mechanics, 6th Edition, McGraw-Hill Companies Inc., 2008.

[15] Z. S. Spakovszky, Unified engineering: Thermodynamics and propulsion, `http://web.mit.edu/16.unified/www/SPRING/propulsion/notes/node86.html`, mIT web course material, Accessed: 2012-11-23.

[16] H. V. Borst, Summary of propeller design procedures and data, volume I, USAAMRDL Technical Report 73-34A, U.S. Army Air Mobility Research and Developement Laboratory, Fort Eustis, Virginia (November 1973).

[17] J. Stack, The compressibility burble, National advisory committee for aeronautics technical note no. 538, Langely Memorial Aeronautical Laboratory, Langley field, Virginia (October 1935).

[18] J. Stack, Tests of airfoils designed to delay the compressibility burble, National advisory committee for aeronautics special report no. 118, Langely Memorial Aeronautical Laboratory, Langley field, Virginia (June 1939).

[19] I. H. Abbott, A. von Doenhoff, Theory of Wing Sections: Including a summary of airfoil data, Courier Dover Publications, 1959.

[20] W. F. Lindsey, D. B. Stevenson, B. N. Daley, Aerodynamics characteristics of 24 NACA 16-series airfoils at Mach numbers between 0.3 and 0.8, NACA technical note no. 1546, Langley Memorial Aeronautical Laboratory, Langley field, Virginia (September 1948).

[21] E. Sand, D. A. Elliot Jr, H. V. Borst, Summary of propeller design procedures and data - volume III, USAAMRDL Technical Report 73-34C, U.S. Army Air Mobility Research and Developement Laboratory, Fort Eustis, Virginia (November 1973).

[22] R.-R. PLC, Gas turbine technology - introduction to a jet engine, `http://www.rolls-royce.com/Images/gasturbines_tcm92-4977.pdf`, Accessed: 2012-01-22 (December 2007).

[23] Aicraft Licence - Propeller Fundamentals, `http://aircraft-license.com/Demo/17.pdf`, Accessed: 2011-10-09.

[24] T. Dahlberg, Procedure to calculate deflections of curved beams, International Journal of Engineering Education.

[25] K. Q. Pan, J. Y. Liu, Geometric nonlinear formulation for curved beams with varying curvature, Theoretical and Applied Mechanics letters 2, 063006.

[26] S. Lenci, F. Clementi, Simple mechanical model of curved beams by a 3d approach, Journal of Engineering Mechanics.

[27] D. P. Raymer, Aircraft Design: A conceptual approach, 3rd Edition, American Institute of Aeronautics and Astronautics, 1999.

[28] UIUC Propeller Database, `http://www.ae.illinois.edu/m-selig/props/propDB.html`, Accessed: 2012-11-04.

[29] J. B. Brandt, M. S. Selig, Propeller performance data at low reynolds numbers, AIAA 2011 – 1255, Department of Aerospace Engineering, Univeristy of Illinois at Urbana-Champaign (January 2011).

[30] G. K. Yamauchi, W. Johnson, Trends of reynolds number effects on two-dimensional airfoil characteristics for helicopter rotor analyses, NASA technical memorandum 84363, Ames Research Center, Moffett Field, California (April 1983).

[31] J. Roskam, C.-T. E. Lan, Airplane Aerodynamics and Performance, 3rd Edition, Design Analysis and Research Corporation, 2003.

[32] W. Amatt, W. E. Bates, H. V. Borst, Summary of propeller design procedures and data, volume II, USAAMRDL Technical Report 73-34B, U.S. Army Air Mobility Research and Developement Laboratory, Fort Eustis, Virginia (November 1973).

[33] M. Drela, Unified engineering I, II, III & IV: Area and bending inertia of airfoil sectionsMIT course material, Accessed: 2013-02-02.

[34] Digital Mechanics, Products and services - Rapid Prototyping, `http://www.digitalmechanics.se/prototyping.php`, Accessed: 2013-02-03.

Source: J.C. Mankins, *"Technology Readiness Level - a white paper"; Office of Space Access and Technology, NASA*

(12) INTERNATIONAL APPLICATION PUBLISHED UNDER THE PATENT COOPERATION TREATY (PCT)

(19) World Intellectual Property Organization
International Bureau

(43) International Publication Date
7 July 2011 (07.07.2011)

PCT

(10) International Publication Number
WO 2011/081577 A1

(51) International Patent Classification:
B64C 11/16 (2006.01) *B64C 11/48* (2006.01)

(21) International Application Number:
PCT/SE2009/000539

(22) International Filing Date:
28 December 2009 (28.12.2009)

(25) Filing Language: English

(26) Publication Language: English

(71) Applicant *(for all designated States except US)*: **VOLVO AERO CORPORATION** [SE/SE]; S-461 81 Trollhättan (SE).

(72) Inventors; and
(75) Inventors/Applicants *(for US only)*: **AVELLAN, Richard** [SE/SE]; Sävenäsgatan 3B, S-416 72 Göteborg (SE). **LUNDBLADH, Anders** [SE/SE]; Mångatan 4, S-461 59 Trollhättan (SE).

(74) Agent: **FRÖHLING, Werner**; Volvo Technology Corporation, Corporate Patents, 06820, M1.7, S-405 08 Göteborg (SE).

(81) Designated States *(unless otherwise indicated, for every kind of national protection available)*: AE, AG, AL, AM, AO, AT, AU, AZ, BA, BB, BG, BH, BR, BW, BY, BZ, CA, CH, CL, CN, CO, CR, CU, CZ, DE, DK, DM, DO, DZ, EC, EE, EG, ES, FI, GB, GD, GE, GH, GM, GT, HN, HR, HU, ID, IL, IN, IS, JP, KE, KG, KM, KN, KP, KR, KZ, LA, LC, LK, LR, LS, LT, LU, LY, MA, MD, ME, MG, MK, MN, MW, MX, MY, MZ, NA, NG, NI, NO, NZ, OM, PE, PG, PH, PL, PT, RO, RS, RU, SC, SD, SE, SG, SK, SL, SM, ST, SV, SY, TH, TJ, TM, TN, TR, TT, TZ, UA, UG, US, UZ, VC, VN, ZA, ZM, ZW.

(84) Designated States *(unless otherwise indicated, for every kind of regional protection available)*: ARIPO (BW, GH, GM, KE, LS, MW, MZ, NA, SD, SL, SZ, TZ, UG, ZM, ZW), Eurasian (AM, AZ, BY, KG, KZ, MD, RU, TJ, TM), European (AT, BE, BG, CH, CY, CZ, DE, DK, EE, ES, FI, FR, GB, GR, HR, HU, IE, IS, IT, LT, LU, LV, MC, MK, MT, NL, NO, PL, PT, RO, SE, SI, SK, SM, TR), OAPI (BF, BJ, CF, CG, CI, CM, GA, GN, GQ, GW, ML, MR, NE, SN, TD, TG).

Published:

— *with international search report (Art. 21(3))*

(54) **Title**: AIR PROPELLER ARRANGEMENT AND AIRCRAFT

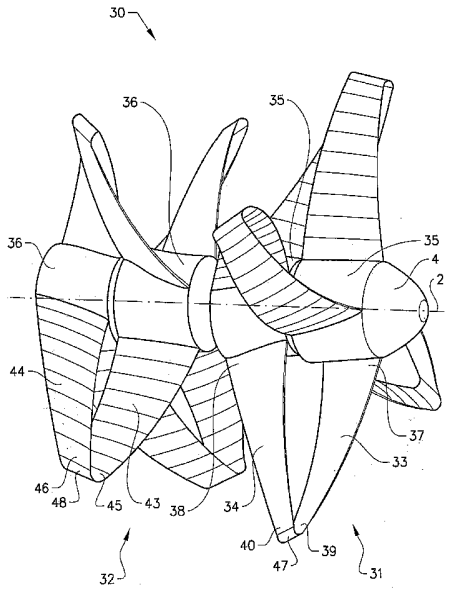

FIG. 3a

(57) **Abstract**: The invention concerns an air propeller arrangement (10, 30, 50) for propulsion of a fixed-wing aircraft (8), said arrangement comprising a first air propeller (11, 31, 51) that comprises a first hub member (15, 35, 55) and at least a first and a second propeller blade (13, 14, 33, 34, 53, 54), said first and second blades (13, 14, 33, 34, 53, 54) being configured to contribute significantly to said propulsion and having a substantially equal length, wherein each of said blades (13, 14, 33, 34, 53, 54) has an inner, root end (17, 18, 37, 38, 57, 58) arranged at the first hub member (15, 35, 55) and an outer, tip end (19, 20, 39, 40, 59, 60) positioned at a distance from the first hub member (15, 35, 55) such that each blade (13, 14, 33, 34, 53, 54) extends in a radial direction from the first hub member (15, 35, 55). The invention is characterized in that the first and second blades (13, 14, 33, 34, 53, 54) are interconnected at their outer ends (19, 20, 39, 40, 59, 60). The invention also concerns an aircraft (8) provided with such an air propeller arrangement (10, 30, 50).

WO 2011/081577 A1

```
%=========================================================================
%   BOX-BLADED PROPELLER DESIGN CODE
%=========================================================================
% PURPOSE
%   - The code generates a box-blade geometry from user inputs starting with
%     a stacking line. Thereafter, flow conditions can be specified and local
%     propeller profiles computed and stacked.
%   - Aerodynamic analysis can be performed for both static and dynamic cases
%   - The mechanical assessment will perform a simple static calculations of
%   the forces and related stresses on the propeller blade
%
% LIST OF SUBFUNCTIONS
%=========================================================================
%   GEOMETRY GENERATION MODULE (in order of implementation)
%=========================================================================
%   - BB_StackingLine:          Generates the box-blade stacking line
%   - BB_BladeSectionGeometry: Computes chord, thickness and design lift
%                               coefficient distributions
%   - BB_DesignPoint:           Defines the Aerodynamic Design point (ADP)
%   - BB_ProfileGenerator:      Generates the box-blade profiles
%   - BB_StackPlot:             Plots the genereted geometry
%   - BB_ProfileOutput:         Outputs profiles for use in CAD software
%-------------------------------------------------------------------------
%=========================================================================
%   AERODYNAMIC ANALYSIS MODULE (in order of implementation)
%=========================================================================
%   STATIC ANALYSIS
%   - BB_AeroStatic:         Aerodynamic analysis under static conditions
%   - BB_AeroStaticPlot:     Plots the results from the static analysis
%   - BB_AeroStaticOutput:   Outputs the static analysis results
%
%   DYNAMIC ANALYSIS
%   - BB_AeroDynamic:         Aerodynamic analysis under dynamic conditions
%   - BB_AeroDynamicPlot:     Plots the results from the dynamic analysis
%   - BB_AeroDynamicOutput:   Outputs the dynamic analysis results
%-------------------------------------------------------------------------
%=========================================================================
%   MECHANICAL ASSESSMENT MODULE (in order of implementation)
%=========================================================================
%   - BB_MechForces:    Computes the shear forces, stresses and safety
%                       factor for the chosen material
%   - BB_MechMoments:   Computes the tipping moment w.r.t the axis
%                       connecting the blade roots. Also includes code
%                       to calculate cross-sectional moments, but it is
%                       not thought to be executed correctly
%
%=========================================================================
%   WRITTEN BY: Samuel Adriansson
%   CONTACT:    samuel.adriansson[at]gmail.com
%   LAST MODIFIED: 2013-02-27
%=========================================================================

clc
clear all
clf
```

```
close all


disp('------------------------------------------------------------')
disp('================== BOX BLADE DESIGN CODE ===================')
disp('------------------------------------------------------------')
disp('MMMMMMMMMMMMMMMMMMMMMMMMMMMMMMMMMMMMMMMMMMMMMMMMMMMMMMMMMMM')
disp('MMMMMMMMMMMMMMMMMMMMMMMMMMMMMMM  NMMMMMMMMMMMMMMMMMMMMMMMM')
disp('MMMMMMMMMMMMMMMMMMMMMMMMMMMMMM7 .M .MMMMMMMMMMMMMMMMMMMMMM')
disp('MMMMMMMMMMMMMMMMMMMMMMMMMMMMMZ  .M . MMMMMMMMMMMMMMMMMMMMM')
disp('MMMMMMMMMMMMMMMMMMMMMMMMMMMM.. MM...MMMMMMMMMMMMMMMMMMMMM')
disp('MMMMMMMMMMMMMMMMMMMMMMMMMMMM ..MM$..MMMMMMMMMMMMMMMMMMMMM')
disp('MMMMMMMMMMMMMMMMMMMMMMMMMMM..7MM$..MMMMMMMMMMMMMMMMMMMMM')
disp('MMMMMMMMMM  .MMMMMMMMMMMMMM. MMM$. MMMMMMMMMMMMMMMMMMMMM')
disp('MMMMMMMMM:  .  MMMMMMMMMMM.MMMM$ MMMMMMMMMMMMMMMMMMMMMMM')
disp('MMMMMMMMM    . ..MMMMMMMMM MMMMMMMMMMMMMMMMMMMMMMMMMMMM')
disp('MMMMMMMMM.   .   . MMMMMMMOM=M.......MMMMMMMMMMMMMMMMMMM')
disp('MMMMMMMMMM ...,. .....MMM  .M..........M....NMMMMMMMMMMM')
disp('MMMMMMMMMMM....M.......IM..N..... .......M. MMMMMMMMMMMM')
disp('MMMMMMMMMMMM ... M..... M M.....  ........M..... MMMMMMMM')
disp('MMMMMMMMMMMMM .....:M....M.....MMMM ....M........MMMMMMMM')
disp('MMMMMMMMMMMMMMM. ....M MMN....M. MM  ............MMMMMMMM')
disp('MMMMMMMMMMMMMMMM+.. ..M......MM.M~,MM.......MMI..MMMMMMMM')
disp('MMMMMMMMMMMMMMMMMMM....M.......MM.MM$....  .MMMMMMMMMMMMM')
disp('MMMMMMMMMMMMMMMMMMMM. .....=..MO=M ..M M.  MMMMMMMMMMMMMM')
disp('MMMMMMMMMMMMMMMMMMMM........M.....MMM~. .?MMMMMMMMMMMMMMM')
disp('MMMMMMMMMMMMMMMMMMMM..M.....M.....M:~ ..MMMMMMMMMMMMMMMM')
disp('MMMMMMMMMMMMMMMMMMMM...Z  ....MMZMM7,....MMMMMMMMMMMMMMM')
disp('MMMMMMMMMMMMMMMMMMMM .........  .  .... MMMMMMMMMMMMMMM')
disp('MMMMMMMMMMMMMMMMMMM............MM.........MMMMMMMMMMMMMM')
disp('MMMMMMMMMMMMMMMMMM.............MMMM........MMMMMMMMMMMMM')
disp('MMMMMMMMMMMMMMMM. .............MMMMMM.......MMMMMMMMMMMM')
disp('MMMMMMMMMMMM .................MMMMMMM=..... MMMMMMMMMMMM')
disp('MMMMMMMMMMMM..............MMMMMMMMMM.....MMMMMMMMMMMMMM')
disp('MMMMMMMMMMMMMM.........MMMMMMMMMMMMMM....NMMMMMMMMMMMMM')
disp('MMMMMMMMMMMMMMMMMMMMMMMMMMMMMMMMMMMMMMM.....MMMMMMMMMMMM')
disp('MMMMMMMMMMMMMMMMMMMMMMMMMMMMMMMMMMMMMMMM....MMMMMMMMMMMM')
disp('MMMMMMMMMMMMMMMMMMMMMMMMMMMMMMMMMMMMMMMM.MMMMMMMMMMMMMMM')
disp('MMMMMMMMMMMMMMMMMMMMMMMMMMMMMMMMMMMMMMMMMMMMMMMMMMMMMMMM')
disp('------------------------------------------------------------')
disp('================== BOX BLADE DESIGN CODE ===================')
disp('------------------------------------------------------------')


%% ========================================================================
%                          GEOMETRY DESIGN MODULE
% ========================================================================
% Stacking line subroutine

disp('------------------------------------------------------')
disp('============= INITIATING GEOMETRIC MODULE ============')
disp('------------------------------------------------------')

check = 1;
```

```
while check == 1
    % Computes the stacking line from user inputs
    [D nstep Rhub Rtip Rhub_real B Xstack s Ap...
        dl StackLength RadStack lowbnd highbnd]  = BB_StackingLine();

    disp('-------------------------------------------------------')
    disp('================ Stacking line generated ==============')

    Q1 = input('Stacking line OK? [Y/N]:','s');

    % Restarts stacking line subroutine if user want to change stacking
    % line
    if Q1 == 'Y'
        check = 0 ;
    else
        check = 1;
    end
end

% Defining chord, thickness and design lift coefficient distributions
[chord t cld chordstring thickstring cldstring AFstring] = ...
 BB_BladeSectionGeometry(D,B,nstep,s,StackLength,RadStack,lowbnd,highbnd);

% Define Aerodynamic design point and set geometry

% Position of stacking line points relative to the leading edge of the chord lines
mu = 0.5;

[beta gamma Xlead Xtrail UnitTangent UnitVrel ...
    UnitProfileNormal RPM Tipspeed RadStack RadLead RadTrail...
    ChordVector ThickVector J_design] = BB_DesignPoint(D,Xstack,s,nstep,chord,mu);

% Generate profiles and stack along stacking line
ProfileCoordinates = zeros(38,3,nstep);
ProfileArea = zeros(nstep,1);
Xcg = zeros(nstep,3);
zbar = zeros(nstep,1);
I_profile = zeros(nstep,1);

for i=1:nstep
    [Xcoord Ycoord Zcoord ProfileArea(i) Xcg(i,:) zbar(i) I_profile(i)] = ...
        BB_ProfileGenerator(mu,t(i),cld(i),chord(i),Xstack(i,:),...
        ChordVector(i,:),ThickVector(i,:),UnitProfileNormal(i,:));

    ProfileCoordinates(:,:,i) = [Xcoord Ycoord Zcoord];
end
disp('-------------------------------------------------------')
disp(' Limiting factor for from the chosen design parameters  ')
disp('-------------------------------------------------------')

%Limiting factor for from the chosen design parameters
FirstRadius = sqrt(ProfileCoordinates(:,2,1).^2 + ProfileCoordinates(:,3,1).^2);
LastRadius = sqrt(ProfileCoordinates(:,2,1).^2 + ProfileCoordinates(:,3,1).^2);

MaxBaseRad = max(max([FirstRadius LastRadius]));
```

```
TipPoint = ceil(nstep/2);
sprintf('Tip profile max thickness: %.3f mm',t(TipPoint)/100*chord(TipPoint)*1000);
sprintf('Tip profile chord: %.3f mm',chord(TipPoint)*1000);
sprintf('Maximum base profile radius (should not exceed %.3f mm ): %.3f mm',↙
Rhub_real*1000,MaxBaseRad *1000);



% Plot stacked profiles
BB_StackPlot(ProfileCoordinates,Xstack,Xlead,Xtrail,nstep)

% Output profiles
BB_ProfileOutput(ProfileCoordinates,nstep,chordstring,thickstring,cldstring,AFstring)

disp('------------------------------------------------------')
disp('================ GEOMETRIC MODULE DONE ================')
disp('------------------------------------------------------')

%% ====================================================================
%                          AERODYNAMIC ANALYSIS MODULE
% ====================================================================

disp('------------------------------------------------------')
disp('======== INITIATING AERODYNAMIC ANALYSIS MODULE ========')
disp('------------------------------------------------------')
disp('1 -> Static analysis) (SSR)');
disp('2 -> Dynamic analysis (DDR)');
disp('3 -> Skip aerodynamic analysis');
analysis = input('Choose analysis type: ');

% Performing static or dynamic analysis
if analysis == 1

    [PerformanceData DataOut RotationalVelocity] = ...
        BB_AeroStatic(nstep,D,B,RPM,chord,cld,t,Xstack,Xlead,...
        UnitTangent,Ap,StackLength,lowbnd,highbnd);

    % Plot performance results
    Q1 = input('Would you like to plot the aerodynamic results? [Y/N]:','s');

    if Q1 == 'Y'
        BB_AeroStaticPlot(RotationalVelocity,PerformanceData,DataOut,...
            chordstring,thickstring,cldstring,AFstring)
    end

    BB_AeroStaticOutput(RotationalVelocity,PerformanceData,DataOut,...
        chordstring,thickstring,cldstring,AFstring)


elseif analysis == 2

    [PerformanceData DataOut InflowVector] = ...
        BB_AeroDynamic(nstep,D,B,RPM,chord,cld,t,Xstack,Xlead,...
        UnitTangent,Ap,StackLength,lowbnd,highbnd);
```

```
    % Plot performance results
    Q1 = input('Would you like to plot the aerodynamic results? [Y/N]:','s');

    if Q1 == 'Y'
        BB_AeroDynamicPlot(InflowVector,PerformanceData,DataOut,...
            chordstring,thickstring,cldstring,AFstring)
    end

    BB_AeroDynamicOutput(InflowVector,PerformanceData,DataOut,...
        chordstring,thickstring,cldstring,AFstring)

elseif analysis == 3
    disp('Skipping mechanical assessment...');

else
    error('Something went wrong, use the correct input');
end
disp('-------------------------------------------------------')
disp('======== AERODYNAMIC ANALYSIS MODULE DONE ========')


%% ========================================================================
%                       MECHANICAL ASSESSMENT MODULE
% ========================================================================

disp('-------------------------------------------------------')
disp('======= INITIATING MECHANICAL ASSESSMENT MODULE ========')
disp('-------------------------------------------------------')
disp('1 -> Material: ULTEM 9085');
disp('2 -> Material: VeroGrey');
disp('3 -> Specifiy material parameters');
disp('4 -> Skip mechanical analysis');
material = input('Choose material: ');

% Mechanical force module

if material == 1
    % Blade density
    rho_blade = 1340; % [kg/m^3]
    % Ultimate tensile strength
    SigmaUTS = 72e6; % [MPa]
    matstring = 'ULTEM9085';

    % Initiate Mechanical forcemodule
    [Fc_total SF] = BB_MechForces(D,B,Xcg,s,nstep,ProfileArea,...
        UnitTangent,UnitProfileNormal,ChordVector,...
        rho_blade,SigmaUTS,RPM,matstring,chordstring,thickstring,...
        cldstring,AFstring);

elseif material == 2
    % Blade density
    rho_blade = 1100;
    % Ultimate tensile strength
    SigmaUTS = 60e6; % [MPa]
```

```
    matstring = 'VeroGrey';

    % Initiate Mechanical force  module
    [Fc_total SF] = BB_MechForces(D,B,Xcg,s,nstep,ProfileArea,...
        UnitTangent,UnitProfileNormal,ChordVector,...
        rho_blade,SigmaUTS,RPM,matstring,chordstring,thickstring,...
        cldstring,AFstring);

elseif material == 3
    matstring = input('Specify the name of the material: ','s')
    rho_blade = input('Specify material density [kg/m^3]: ');
    SigmaUTS = input('Specify ultimate tensile strength of the material [Pa]: ');


    % Initiate Mechanical force module
    [Fc_total SF] = BB_MechForces(D,B,Xcg,s,nstep,ProfileArea,...
        UnitTangent,UnitProfileNormal,ChordVector,...
        rho_blade,SigmaUTS,RPM,matstring,chordstring,thickstring,...
        cldstring,AFstring);

elseif material == 4
    disp('Skipping mechanical analysis...');
else
    error('Something went wrong, use the correct input')
end

% Mechanical moments module
% Calculates mechanical moments (THEORY MUST BE VERIFIED)

% BB_MechMoments(D,B,Xcg,s,nstep,ProfileArea,...
%     UnitTangent,UnitProfileNormal,ChordVector,...
%     rho_blade,SigmaUTS,RPM,matstring,chordstring,thickstring,...
%     cldstring,AFstring,I_profile);



disp('-----------------------------------------------------')
disp('========== MECHANICAL ASSESSMENT MODULE DONE ==========')
disp('-----------------------------------------------------')
```